Inorganic Chemistry
Cite This: Inorg. Chem. 2019, 58, 3175−3188
Article
pubs.acs.org/IC

Theoretical Studies on Hexanuclear $[M_3(\mu_3\text{-O/OH})]_2$ (M = Fe(III), Mn(III), and Ni(II)) Clusters: Magnetic Exchange, Magnetic Anisotropy, and Magneto-Structural Correlations

Mukesh Kumar Singh and Gopalan Rajaraman*

Department of Chemistry, Indian Institute of Technology Bombay, Powai, Mumbai, Maharashtra, India-400076

Supporting Information

ABSTRACT: Controlling spin Hamiltonian parameters such as magnetic exchange and magnetic anisotropy of polynuclear clusters is of great interest in the area of single molecule magnets (SMMs). Among large polynuclear clusters, hexanuclear clusters offer the best compromise in terms of size as they are often rigid, solution stable, and chemically amenable. The $\{M_6O_2\}$ core is one of the common architectures known for many hexanuclear clusters and generally reported to possess a diamagnetic $S_T = 0$ spin ground state, barring a few exceptions. In these clusters, there are several open questions that are poorly understood: (a) What controls the nature of magnetic exchange, which in turn dictates the ground state spin values? (b) For clusters possessing a nonzero spin ground state, what dictates the magnetic anisotropy? Here, using density functional methods, we have attempted to shed light on these two question by evaluating the exchange coupling constants in $[Fe_6^{III}O_2(OH)_2\{(C_4N_2H_2SMe)_2C(OH)\text{-}O\}_2(^tBuCO_2)_{10}]$ (**1**), $[Fe_6^{III}(O)_2(O_2CH_2)(O_2CCH_2{}^tBu)_{12}(py)_2]$ (**2**), $[Fe_6^{III}(O_2)\text{-}(O)_2(O_2CCMe_3)_{12}(py)_2]$ (**3**), $[Fe^{III}{}_6O_3(O_2CMe)_9(OEt)_2(bpy)_2]ClO_4$ (**4**), $[Mn^{III}{}_6O_2(O_2CH_2)(O_2CPe^t)_{11}(HO_2CPe^t)_2(O_2CMe)]$ (**5**), and $[Ni^{II}{}_6(OH)_4(O_2C{}^tBu)_8(^tBuCO_2H)_4]$ (**6**) complexes. We have estimated all the eight near-neighbor exchange coupling constants in these clusters. Our calculations not only agree with the experimental results but also offer insight on the origin of the spin ground state. Extensive magneto-structural correlations developed by varying M−O−M angles and M−O distances reveal that J values are extremely sensitive to small structural distortions. Correlations developed indicate that both the parameters are important for Fe(III), but for Mn(III) and Ni(II), the angles were found to play a dominant role. Quite interestingly, the computed zero-field splitting parameter $D_{S=5}$ of complex **1** reveals that the exchange contribution to the anisotropy controls the sign of the ground state D value—an observation which differs from the general perception that the ground state D is controlled by the single-ion zero-field splitting parameter.

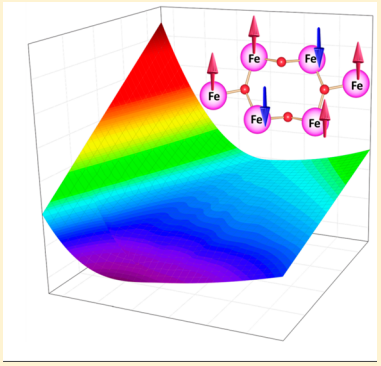

INTRODUCTION

The oxo-bridged triangular $\{M_3O\}$ units (here, M = Fe(III), Mn(III), and Ni(II)) are of fundamental interest as they are the building units in some minerals,[1] metallo enzymes,[2] metal storage proteins such as ferritin,[3] and higher nuclearity clusters.[4] They are also active centers for many catalytic transformations[5] and can exhibit fascinating magnetic properties such as single-molecule magnets (SMMs).[6,7] This discovery of SMM properties with $[Mn_{12}O_{12}(OAc)_{16}\text{-}(H_2O)_4]\cdot 2HOAc\cdot 4H_2O$ "Mn_{12} acetate"[8] offers tantalizing applications such as high density molecular information storage devices.[9] In addition to "Mn_{12} acetate," the other extensively studied SMM belongs to the Fe_8 system, $[Fe_8O_8(OH)_{12}(tacn)_6]Br_8\cdot 9H_2O$ (tacn = 1,4,7-triazacyclononane), both with an $S_T = 10$ ground state.[10] The latter was the first oxo-hydroxo bridged Fe(III) complex having a nuclearity higher than three. In order to mimic the ferritin core, a crystal of the family $[Fe^{III}{}_{19}]$ has been synthesized within a pair of cocrystallized Fe_{17}/Fe_{19} species having a molecular formula of $[Fe_{19}(metheidi)_{10}(OH)_4O_6(H_2O)_{12}](NO_3)\cdot 24H_2O$.[11]

Among all the reported polynuclear complexes in the past two decades,[12−14] the complexes based on Fe(III), Mn(III), and Ni(II) gain much attention essentially due to two reasons: (i) The Fe(III) ion offers the largest single-site spin in transition metals, leading to large spin clusters (very large spin ground states as high as $S_T = 45$ are reported with Fe(III)).[15] (ii) Mn(III) and Ni(II) ions, on the other hand, offer large anisotropy—an important ingredient for SMMs (very large D values as high as -500 cm^{-1} are reported for Ni(II) systems).[16] While the magnetic exchange and the associated magnetic anisotropy of these ions are studied using various dinuclear and trinuclear systems,[17,18] there are very few studies on how these magnetic properties translate as we move from basic trinuclear $\{M_3O\}$ units to higher nuclearity clusters. While there are numerous studies on larger polymetallic clusters, these clusters are often made serendipitously and hence do not offer chemical control on structural alterations that are desired to regulate the magnetic properties.[15,19]

Hexanuclear complexes seem to be the best compromise at this juncture, as they have two $\{M_3O\}$ units, and often these clusters are rigid, solution stable, and chemically amena-

Received: November 21, 2018
Published: February 11, 2019

DOI: 10.1021/acs.inorgchem.8b03257
Inorg. Chem. 2019, 58, 3175−3188

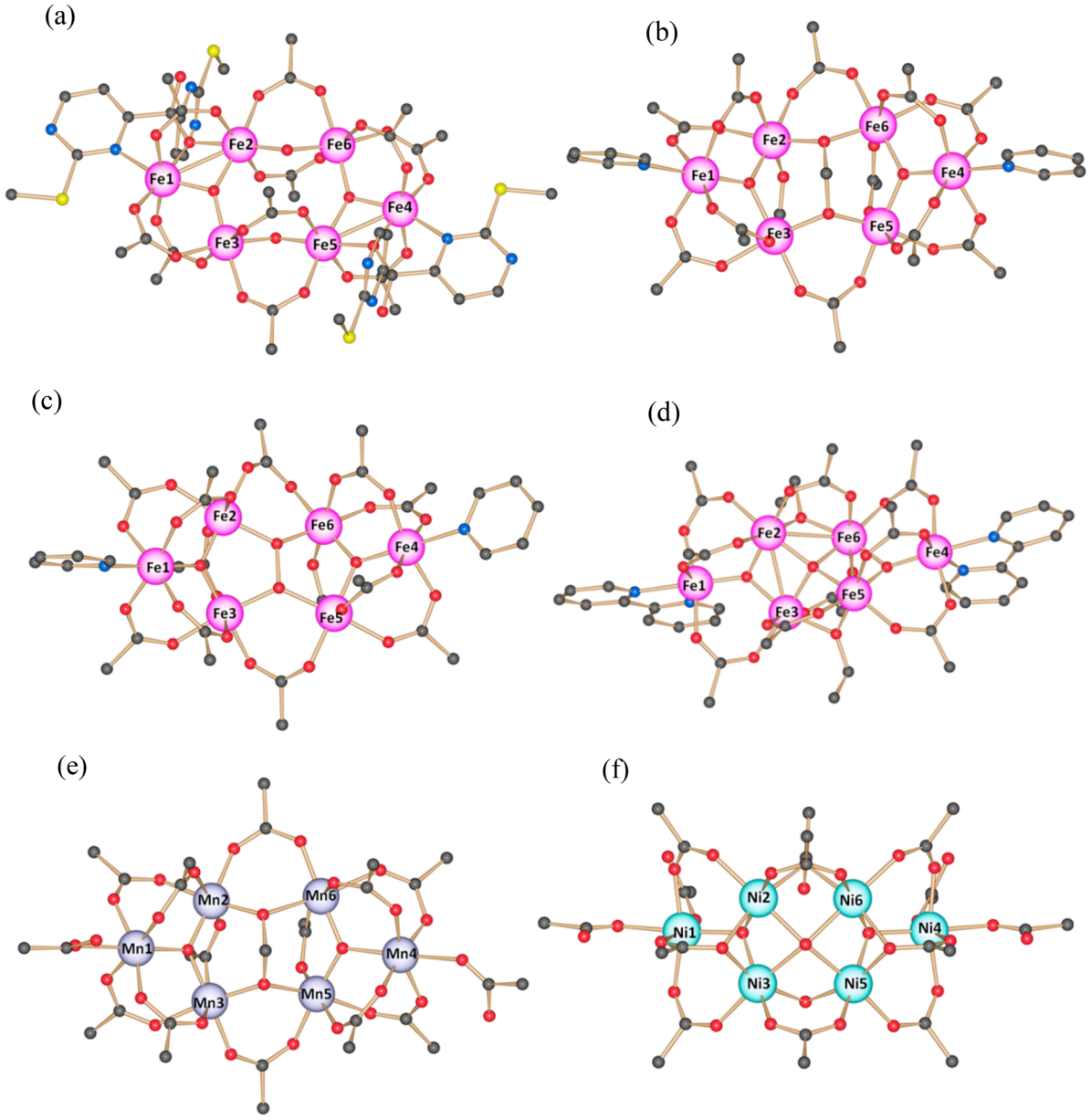

Figure 1. X-ray crystal structures of complexes (a) **1**, (b) **2**, (c) **3**, (d) **4**, (e) **5**, and (f) **6**. $3CH_3$ groups are removed from each $^tBuCO_2$ for clarity; all H atoms are removed for clarity. Scheme: pink (Fe), purple (Mn), cyano-green (Ni), yellow (S), black (C), blue (N), and red (O).

ble.[12b,14a,b,d,e] A very good example here would be the report of the $\{Mn^{III}_6\}$ cluster, possessing an $S = 12$ ground state, with a record high effective energy barrier of 62 cm^{-1}.[12b,13] This structure is very robust, and various modifications and magneto-structural correlations have been experimentally probed for this architecture. Motivated by these studies and the corresponding architecture, here we intend to look for structurally analogous $\{M_6O_2\}$ clusters of Fe(III), Mn(III), and Ni(II) to understand the nature of magnetic coupling and the associated magnetic anisotropy. In this regard, reports of several complexes with the $\{Fe_6O_2\}$ core and differing ground state S_T values grabbed our attention. Particularly, there are two classes of such clusters, with some clusters reported to possesses an $S_T = 5$ ground state while others have an $S_T = 0$ ground state.[14a,c,20] Structurally analogous Mn(III) and Ni(II) clusters are also reported for this architecture. Hence, we decided to undertake a detailed computational investigation on six different hexanuclear clusters to understand the underlying exchange coupling pattern and also the anisotropy. For this study, we have chosen $[Fe^{III}_6O_2(OH)_2\{(C_4N_2H_2SMe)_2C(OH)O\}_2(^tBuCO_2)_{10}]$ **1**,[14a] $[Fe^{III}_6(O)_2(O_2CH_2)(O_2CCH_2{}^tBu)_{12}(py)_2]$ **2**,[14b] $[Fe^{III}_6(O_2)(O)_2(O_2CCMe_3)_{12}(py)_2]$ **3**,[14n] $[Fe_6O_3(O_2CMe)_9(OEt)_2(bpy)_2]ClO_4$ **4**,[14c] $[Mn_6O_2(O_2CH_2)(O_2CPe^t)_{11}(HO_2CPe^t)_2(O_2CMe)]$ **5**,[14d] and $[Ni^{II}_6(OH)_4(O_2C^tBu)_8(^tBuCO_2H)_4]$ **6**[14e] complexes (see Figure 1).

The core for all these molecules consists of two $[M3^{III/II}(\mu_3\text{-}O/OH)]$ units. Connectivities of ligands along with the exchange coupling of the metals are shown in Table 1 for complexes **1**–**6**. All complexes have an octahedral environment around their metallic centers. Complexes **1**–**4** have two μ_2-OH^-, one μ_4-($\eta_2\eta_2$-$CH_2O_2{}^{2-}$), one μ_4-($\eta_2\eta_2$-$O_2{}^{2-}$), and one μ_4-O^{2-} bridging group, respectively, between the two triangular $\{Fe_3O\}$ metallic units. Complex **5** is analogous to complex **2** except that the metal center is Mn(III). While the core

DOI: 10.1021/acs.inorgchem.8b03257
Inorg. Chem. 2019, 58, 3175−3188

Table 1. Selected Structural Parameters along with the Corresponding *J* Value Notation for Complexes 1−6

	1			2			3			4			5			6		
		r	*ϕ*		*r*	*ϕ*		*r*	*ϕ*		*r*	*ϕ*		*r*	*ϕ*		*r*	*ϕ*
J_1	μ_3-O^{2-}	1.933	100	μ_3-O^{2-}	1.909	119	μ_3-O^{2-}	1.889	122	μ_3-O^{2-}	1.894	120	μ_3-O^{2-}	1.940	119	μ_3−OH^-	2.021	115
	μ_2-L_1^-			μ_2-A_2			μ_2-A_1			μ_2-A_3			μ_2-A_4			η_2-μ_3-A_1		
	μ_2-A_1			μ_2-A_2			μ_2-A_1			μ_2-A_3			μ_2-A_4			μ_2-A_1		
J_2	μ_3-O^{2-}	1.930	138	μ_3-O^{2-}	1.951	122	μ_3-O^{2-}	1.906	117	μ_3-O^{2-}	1.943	99	μ_3-O^{2-}	1.861	124	μ_3−OH^-	2.044	86
				μ_2-A_2			μ_2-A_1			μ_4-O^{2-}			μ_2-A_4			μ_4-OH^-		
				μ_4-$CH_2O_2^{2-}$			μ_4-O_2^{2-}									η_2-μ_3-A_1		
J_3	μ_3-O^{2-}	1.894	118	μ_3-O^{2-}	1.914	119	μ_3-O^{2-}	1.897	122	μ_3-O^{2-}	1.889	130	μ_3-O^{2-}	1.936	117	μ_3−OH^-	2.018	112
	μ_2-A_1			μ_2-A_2			μ_2-A_1			μ_2-A_3			μ_2-A_4			η_2-μ_3-A_1		
	μ_2-A_1			μ_2-A_2			μ_2-A_1						μ_2-A_4			μ_2-A_1		
J_4	μ_3-O^{2-}	1.933	100	μ_3-O^{2-}	1.909	119	μ_3-O^{2-}	1.894	122	μ_3-O^{2-}	1.891	123	μ_3-O^{2-}	1.951	118	μ_3−OH^-	2.015	113
	μ_2-L_1^-			μ_2-A_2			μ_2-A_1			μ_2-A_3			μ_2-A_4			η_2-μ_3-A_1		
	μ_2-A_1			μ_2-A_2			μ_2-A_1			μ_2-A_3			μ_2-A_4			μ_2-A_1		
J_5	μ_3-O^{2-}	1.930	138	μ_3-O^{2-}	1.951	122	μ_3-O^{2-}	1.909	116	μ_3-O^{2-}	1.945	99	μ_3-O^{2-}	1.843	124	μ_3−OH^-	2.035	86
				μ_2-A_2			μ_2-A_1			μ_4-O^{2-}			μ_2-A_4			μ_4-OH^-		
				μ_4-$CH_2O_2^{2-}$			μ_4-O_2^{2-}									η_2-μ_3-A_1		
J_6	μ_3-O^{2-}	1.894	118	μ_3-O^{2-}	1.914	119	μ_3-O^{2-}	1.902	122	μ_3-O^{2-}	1.886	127	μ_3-O^{2-}	1.957	118	μ_3−OH^-	2.018	114
	μ_2-A_1			μ_2-A_2			μ_2-A_1			μ_2-A_3			μ_2-A_4			η_2-μ_3-A_1		
	μ_2-A_1			μ_2-A_2			μ_2-A_1						μ_2-A_4			μ_2-A_1		
J_7	μ_2−OH^-	1.951	123	μ_2-A_2	1.978	132	μ_2-A_1	2.034	130	μ_2-OEt^-	2.013	98	μ_4-$CH_2O_2^{2-}$	2.015	126	μ_4-OH^-	2.120	93
	μ_2-A_1			μ_4-$CH_2O_2^{2-}$			μ_4-O_2^{2-}			μ_2-A_3			μ_2-A_4			η_2-μ_3-A_1		
	μ_2-A_1									μ_4-O^{2-}						η_2-μ_3-A_1H		
J_8	μ_2−OH^-	1.951	123	μ_2-A_2	1.978	132	μ_2-A_1	2.019	127	μ_2-OEt^-	2.026	97	μ_4-$CH_2O_2^{2-}$	2.001	127	μ_4-OH^-	2.120	91
	μ_2-A_1			μ_4-$CH_2O_2^{2-}$			μ_4-O_2^{2-}			μ_2-A_3			μ_2-A_4			η_2-μ_3-A_1		
	μ_2-A_1									μ_4-O^{2-}						η_2-μ_3-A_1H		

[a] *r* = avg. M−O distance (Å), *ϕ* = M−O−M angle (deg), L1 = DTPK [di-2-(4-methylthio)pyrimidyl-diol], μ_2-A_1 = μ_2-(t-but)COO^-, μ_2-A_2 = μ_2-(t-but)CH_2COO^-, μ_2-A_3 = μ_2-CH_3COO^-, μ_2-A_4 = μ_2-(t-Pe)COO^-.

DOI: 10.1021/acs.inorgchem.8b03257
Inorg. Chem. 2019, 58, 3175−3188

structure of complex **6** is similar to complex **4**, we would like to note here that this is the only structure where −OH instead of −O is bridging the metal ion, making this structure different from the other five complexes.

Magnetic susceptibility studies reveal that complex **1** possesses a ground state of S_T = 5, while all the other complexes have S_T = 0 ground state. The coordination number around metallic centers in all complexes is satisfied primarily by carboxylate groups with additional ligation in some metal centers offered by coligands (in **1**, L_1 = DTPK [di-2-(4-methylthio) pyrimidyl-diol]; in **2** and **3**, pyridine; in **4**, 2,2′-bipyridene; in **4** and **5**, alkoxy groups; and in **6**, hydroxo group). Another major difference between these complexes is that complex **1** has a planar Fe_6 array, whereas complexes **2**, **3**, **5**, and **6** have strong distortions leading to a boat-shaped M_6 topology. For complex **4**, on the other hand, a twisted boat shape topology was detected. Experimental magnetic studies are reported for complexes **1**, **2**, **4**, and **5**. For complexes **3** and **6**, the magnetic properties are reported for a structurally analogous complex, and hence these data are utilized for comparison.[21,22]

In this work, we have undertaken computational studies on all these complexes (**1**−**6**) to specifically answer the following intriguing questions: (i) How reliable are the estimate of J values from DFT calculations in reproducing the susceptibility data and spin ground state (S_T)? (ii) Which structural parameter controls the exchange coupling in these clusters and how they vary as we move from Fe to Mn to Ni? (iii) How does the magnetic anisotropy of S_T = 5 state in complex **1** originate and what are the individual contributions to the anisotropy that yield overall negative D?

COMPUTATIONAL DETAILS

The calculations were performed in the Gaussian 09 suite of programs[23] using the hybrid B3LYP functional.[24] We have used the TZV basis set[25] for all elements. Earlier studies performed on di/polynuclear transition metal complexes using the B3LYP/TZV methodology yielded a good numerical estimate of J values for Fe, Mn, and Ni clusters, offering confidence in the employed methodology.[26,27] In bimetallic systems, it is very simple to calculate the energy differences between the high spin and broken symmetry states. But as the number of metallic centers increases in the systems, the possible numbers of spin configurations as well as numbers of exchange coupling constants are also increased. In our studied systems, the possible number of local spin configurations is 32 ($2^6/2$). Here, we have computed energies of 13 spin configurations on complexes **1**−**6** in order to obtain eight exchange coupling constants for complexes **1**−**3** and **5** and nine exchange coupling constants for complexes **4** and **6**. The computed spin configurations include a high spin solution with all spins up, five solutions with two spins down, six solutions having one spin down, and one solution with three spins up and three spins down, leading to S_T = 0 (all the spin projection ways for different solutions are given in Table S1). We have generated a system of 13 equations with eight/nine unknowns, which are then solved using linear equations and by using the singular value decomposition. In order to check the effect of bridging groups, we have also performed calculations on models.

The Heisenberg−Dirac−van Vleck Hamiltonian[28] is used for the determination and evaluation of the magnetic susceptibility in the form of eq 1 as

$$\hat{H} = -\sum_{ij} 2J_{ij} S_i \cdot S_j \tag{1}$$

We have used PHI for fitting experimental data and for simulating the DFT calculated magnetic susceptibility plots.[29] To estimate the zero-field splitting (zfs) parameters, *ab initio* CASSCF calculations are proven to be valuable.[16,30] However, the application of this method is limited to mono- and dinuclear systems, as such calculations on larger clusters are not possible at this stage. Thus, to estimate the zfs of the S_T = 5 state of **1**, we have utilized DFT methods. While these methods are known to underestimate D in several mononuclear complexes, for larger clusters, they tend to yield a good numerical estimate of D, and this has been shown in many instances.[31] We have used DFT calculations for the estimation of the D and g tensors in the ORCA suite of programs,[32] employing the B3LYP functional using quasi-degenerate theory[33] with a CP approach.[34] The Alhrichs TZVPP basis set was used for the metal ions, while for the remaining atoms we have used the TZVP basis set. The RI approximations were considered during the calculation with an auxiliary TZV/J columbic fitting basis set.[35] Increased integration grids (Grid 5 in ORCA) along with tight SCF convergence were used. The estimated D has both spin−spin and spin−orbit contributions.

RESULTS AND DISCUSSION

Estimation of Magnetic Exchange Interactions in 1−6. Complexes **1**−**3** and **5** have eight distinct magnetic exchange interactions: three within each Fe_3 triangle and two between the ions linking the triangles. The corresponding exchange Hamiltonian is given below in eq 2a. However, complexes **4** and **6** have nine distinct magnetic exchange interactions: three within each Fe_3 triangle and three between the ions linking the triangles. The corresponding exchange Hamiltonian is given below in eq 2b:

$$\begin{aligned}\hat{\mathbf{H}} = &-2J_1(\hat{\mathbf{S}}_1\cdot\hat{\mathbf{S}}_2) - 2J_2(\hat{\mathbf{S}}_2\cdot\hat{\mathbf{S}}_3) - 2J_3(\hat{\mathbf{S}}_1\cdot\hat{\mathbf{S}}_3) - 2J_4(\hat{\mathbf{S}}_4\cdot\hat{\mathbf{S}}_5)\\ &- 2J_5(\hat{\mathbf{S}}_5\cdot\hat{\mathbf{S}}_6) - 2J_6(\hat{\mathbf{S}}_4\cdot\hat{\mathbf{S}}_6) - 2J_7(\hat{\mathbf{S}}_3\cdot\hat{\mathbf{S}}_5) - 2J_8(\hat{\mathbf{S}}_2\cdot\hat{\mathbf{S}}_6)\end{aligned} \tag{2a}$$

$$\begin{aligned}\hat{\mathbf{H}} = &-2J_1(\hat{\mathbf{S}}_1\cdot\hat{\mathbf{S}}_2) - 2J_2(\hat{\mathbf{S}}_2\cdot\hat{\mathbf{S}}_3) - 2J_3(\hat{\mathbf{S}}_1\cdot\hat{\mathbf{S}}_3) - 2J_4(\hat{\mathbf{S}}_4\cdot\hat{\mathbf{S}}_5)\\ &- 2J_5(\hat{\mathbf{S}}_5\cdot\hat{\mathbf{S}}_6) - 2J_6(\hat{\mathbf{S}}_4\cdot\hat{\mathbf{S}}_6) - 2J_7(\hat{\mathbf{S}}_3\cdot\hat{\mathbf{S}}_5) - 2J_8(\hat{\mathbf{S}}_2\cdot\hat{\mathbf{S}}_6)\\ &- 2J_9(\hat{\mathbf{S}}_4\cdot\hat{\mathbf{S}}_5 + \hat{\mathbf{S}}_3\cdot\hat{\mathbf{S}}_6)\end{aligned} \tag{2b}$$

where $\mathbf{S}_i$ are the spin operators of each paramagnetic M(III/II) center and J_{ij} are coupling constants between the magnetic centers.

For all studied complexes, calculated J values are given in Table 2 and Figure 2. Calculated magnetic coupling constants and magnetic susceptibility plots (see Figure 3 and Figure S1) indicate a dominant intramolecular antiferromagnetic coupling in all of these complexes. DFT calculated χT vs T plots for all of these complexes (shown by gray color) along with the experimental data and experimental fits are given in Figure 3. The computed susceptibility fits well with the experimental data, offering confidence in the estimated exchange coupling constants. In complex **1**, all the estimated J values are found to be antiferromagnetic in nature with J_6 being the strongest and J_4 being the weakest exchange. Within the $\{Fe_3O\}$ triangular unit, clearly there are competing interactions. However, as J_2 and J_3 interactions are dominant with J_1 being very weak, this

DOI: 10.1021/acs.inorgchem.8b03257
Inorg. Chem. 2019, 58, 3175−3188

Table 2. B3LYP Computed J (cm^{-1}) Values for Complexes 1−6

J values	1	2	3	4	5	6
J_1	−6.5	−16.4	−36.0	−37.7	−4.8	−18.1
J_2	−31.2	−10.5	−32.4	−0.8	1.8	−3.4
J_3	−40.2	−16.3	−31.6	−42.3	−5.8	−14.3
J_4	−6.0	−16.3	−41.8	−43.6	−8.3	−13.5
J_5	−30.8	−10.4	−31.0	+1.5	−0.6	−3.4
J_6	−40.9	−16.5	−32.1	−38.4	−7.4	−12.8
J_7	−14.5	−7.9	−16.3	−23.4	−1.0	−3.1
J_8	−14.8	−8.1	−17.7	−28.7	−1.4	−5.5
J_9				−36.7		−11.7

results in an $S = 5/2$ ground state within the triangle. The intertriangle (J_7 and J_8) interactions are antiferromagnetic and are noncompeting, leading to the stabilization of the $S_T = 5$ ground state for complex **1**. The DFT computed magnetic coupling values for complex **1** are in accord with the experimental values.[14a] The spin-configuration corresponding to the ground state is shown in Figure 2, and the Eigenvalues of the spin states computed are shown in Figure 4.

As we move from complex **1** to **2**, the J values become significantly smaller, with many interactions turning out to be equal in strength (for example, J_1, J_3, J_4, and J_6), leading to several competing interactions. Within the triangular $\{Fe_3O\}$ unit, the competing interactions lead to spin frustration and, hence, the stabilization of $S = 1/2$ ground state. The coupling of two such triangles leads to an overall spin ground state of $S_T = 0$. As we move from complex **2** to **3**, the strength of the exchange coupling constant is found to enhance; however, the magnitude of the J's within the $\{Fe_3O\}$ triangular units are very similar in strength, leading to a similar situation to complex **2**. Similar to complex **1**, in complex **4** as well, the individual $\{Fe_3O\}$ triangular unit yields an $S = 5/2$ state, as two exchange interactions within the triangle are stronger than the third one (see Figure 2). However, as the structural topology is different, the intertriangle exchange couplings ($J_7/J_8/J_9$) are found to be much stronger, leading to an $S_T = 0$ ground state.

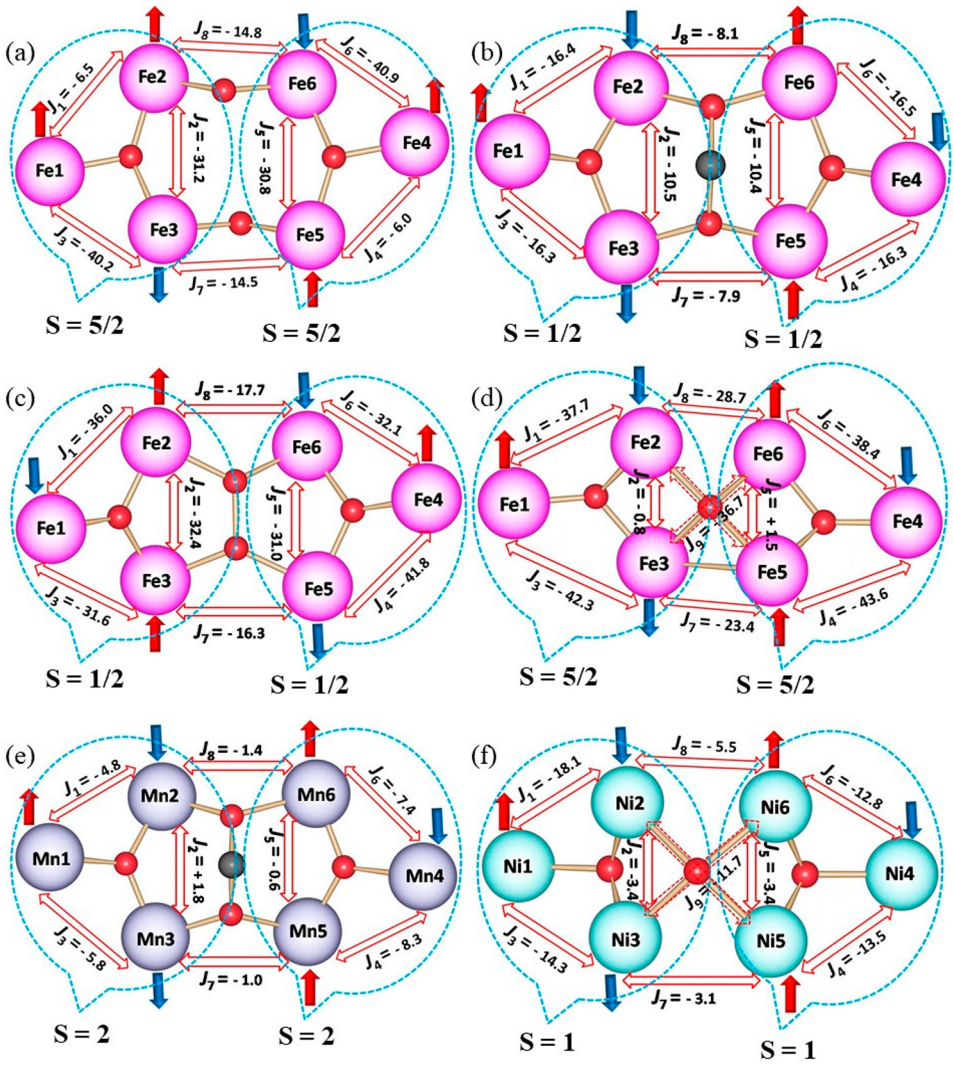

Figure 2. Metallic core structure of complexes **1**−**6** along with DFT computed magnetic coupling constants for complex (a) **1**, (b) **2**, (c) **3**, (d) **4**, (e) **5**, and (f) **6**. The blue dotted circles indicate the ground state S value obtained within the trimetallic unit utilizing the corresponding J values using MAGPACK. The corresponding data for the $\{M_3O\}$ units are given in Figure S2 of the Supporting Information). Error bars for all the calculated values are found to be less than 0.1 cm^{-1}.

DOI: 10.1021/acs.inorgchem.8b03257
Inorg. Chem. 2019, 58, 3175−3188

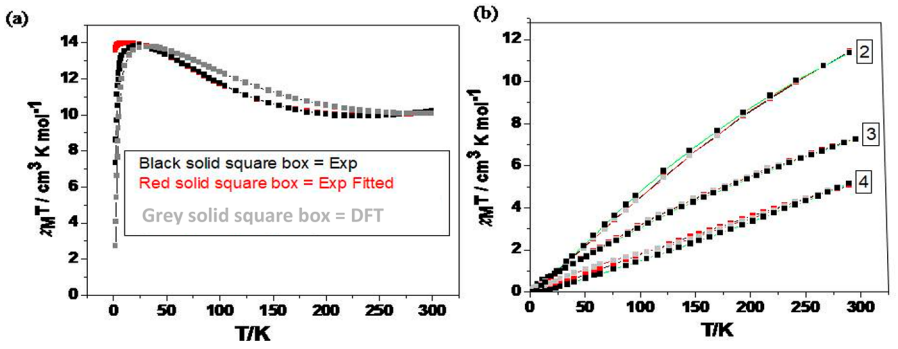

Figure 3. χT vs T plots for complexes (a) **1** and (b) **2**, **3**, and **4**. DFT stimulated plots along with experimental data and fit obtained by the experimentalist are shown.

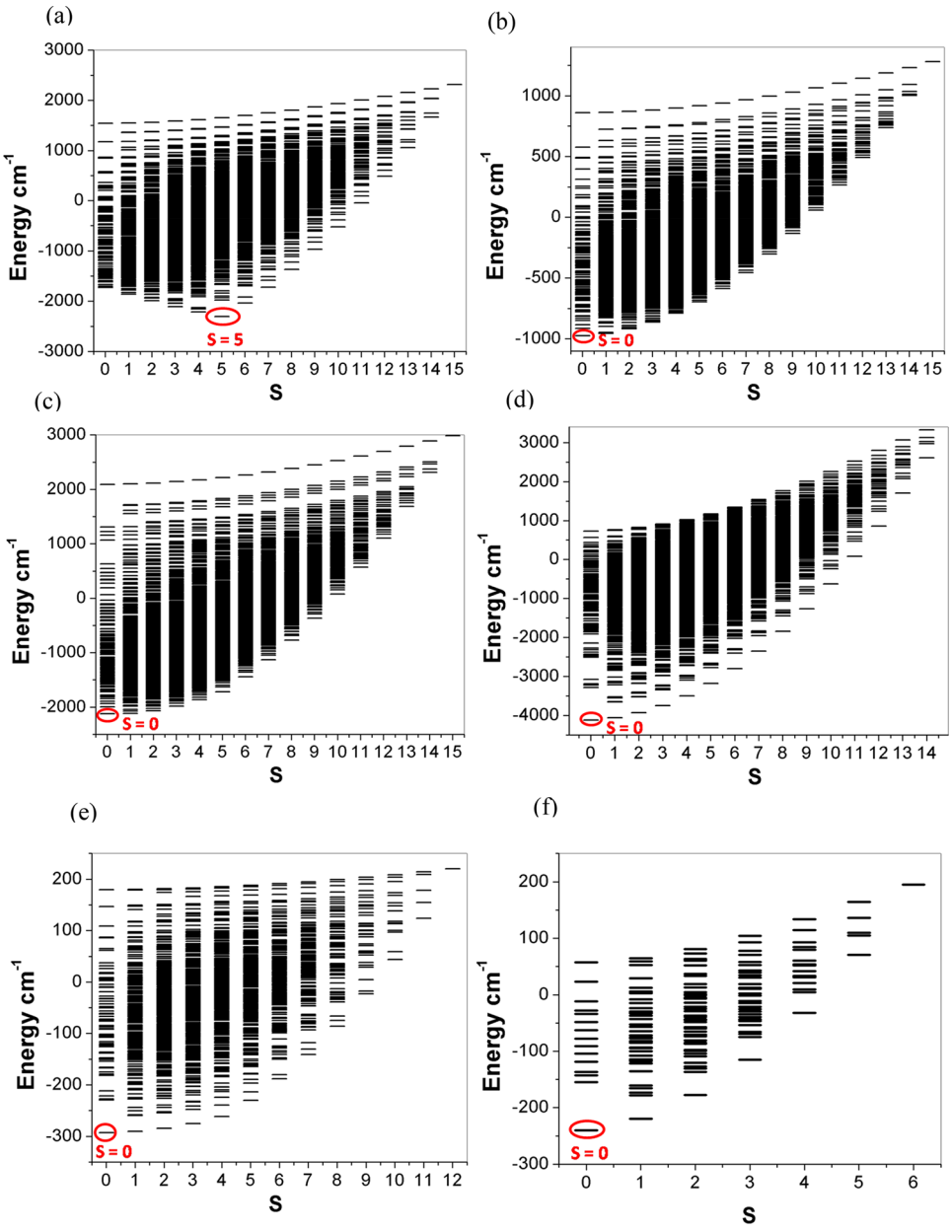

Figure 4. Energies of various spin-states against different S values. The red circles indicate the ground S_T value in each case for complexes (a) **1**, (b) **2**, (c) **3**, (d) **4**, (e) **5**, and (f) **6**.

If we move to complex **5**, a mixture of weak ferro- and antiferromagnetic couplings are detected with each of the $\{Mn_3O\}$ units yielding an $S = 2$ ground state. These two $S = 2$ states couple antiferromagnetically to each other, leading to a

DOI: 10.1021/acs.inorgchem.8b03257
Inorg. Chem. 2019, 58, 3175−3188

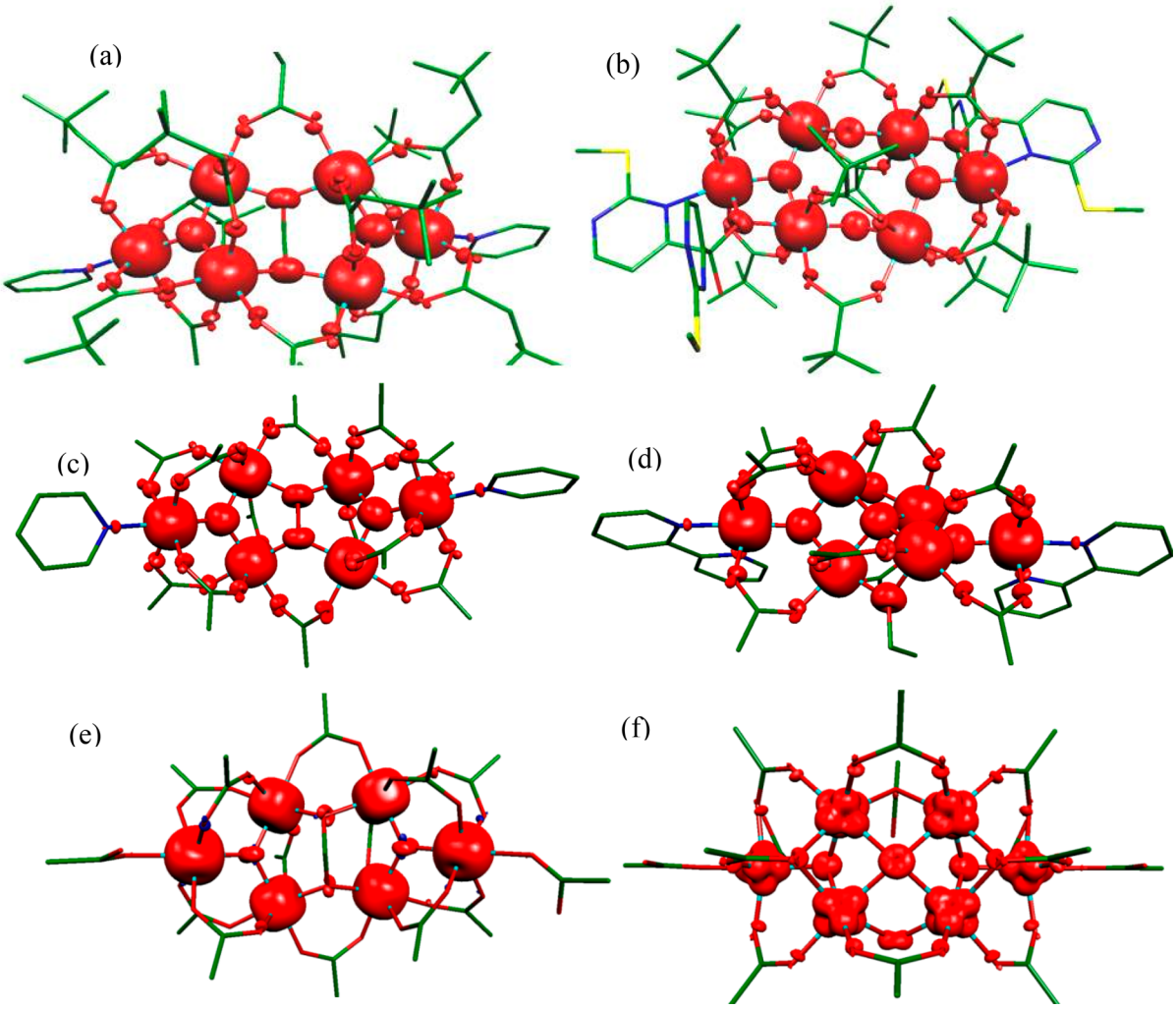

Figure 5. Spin density plots for complexes (a) **1**, (b) **2**, (c) **3**, (d) **4**, (e) **5**, and (f) **6** (hydrogen atoms are omitted for clarity). The iso-density surface shown corresponds to a value of 0.001 e^-/bohr^3.

net S_T = 0 ground state. Complex **6** has antiferromagnetic interaction within the {Ni_3O/OH} triangular unit with J_1/J_4 and J_3/J_6 being larger than J_2/J_5 and hence the stabilization of S = 1 ground state. Between the two triangles, strong antiferromagnetic interactions ($J_7/J_8/J_9$) lead to a net S_T = 0 ground state. From these calculations, it is clear that various factors influence the magnetic exchange coupling constants within {M_6} clusters; stabilization of the nonzero ground state S_T value is possible only when the peripheral exchange coupling constants J_1 and J_3 (or J_4 and J_6} are noncompeting with one exchange being much larger than the other one. If the exchange coupling constants within the triangles are very similar (and are antiferromagnetic), this results in an S_T = 0 ground state, independent of the nature of the metal ions/other exchange coupling constants. Thus, it is important to design ligands that influence exclusively the peripheral exchange coupling constants to obtain nonzero ground state S values. It is also important to note here that the first excited spin state is very close to the ground spin state in most of these complexes owing to spin frustration. Particularly for complex **2**, an S = 1 state was found to lie just 18.9 cm^{-1} above the ground state S = 0, and in fact there are three S = 1 states that lie very close to each other, suggesting spin frustration.

The spin density plot of the high-spin state of complexes **1**−**6** are shown in Figure 5. The Fe(III) centers are found to have a spin density in the range of ∼4.25 to 4.30 ,while Mn(III) centers are found to have a spin density of ∼3.9. Ni(II) centers have a spin density of ∼1.72. Clearly, the extent of delocalization of spins in Fe centers is found to be much larger than that found for the other two metals. For the Fe(III) complex, a large spin density on μ_3-O atoms is detected, while only a little spin density on the same has been detected for the Mn(III) complex. This is essentially due to the difference in spin polarization/delocalization that is promoted by individual ions (see Figure 5 and Table S2).

Magneto-Structural Correlations. Although the bridging groups/atoms between all the metals are found to be the same in all of the complexes, magnetic coupling constant values are found to vary from weak ferromagnetic interaction to relatively large antiferromagnetic interaction. In this instance, magneto-structural correlations can offer a clue to understanding the variation in exchange coupling constants observed among these complexes.[14f] Magneto-structural correlations developed on dinuclear Fe(III) compounds reveal that J is strongly dependent on two structural parameters, the Fe−O bond distances and Fe−O−Fe bond angles. To comprehend how the J's are altered here in these systems, we have decided to

DOI: 10.1021/acs.inorgchem.8b03257
Inorg. Chem. 2019, 58, 3175−3188

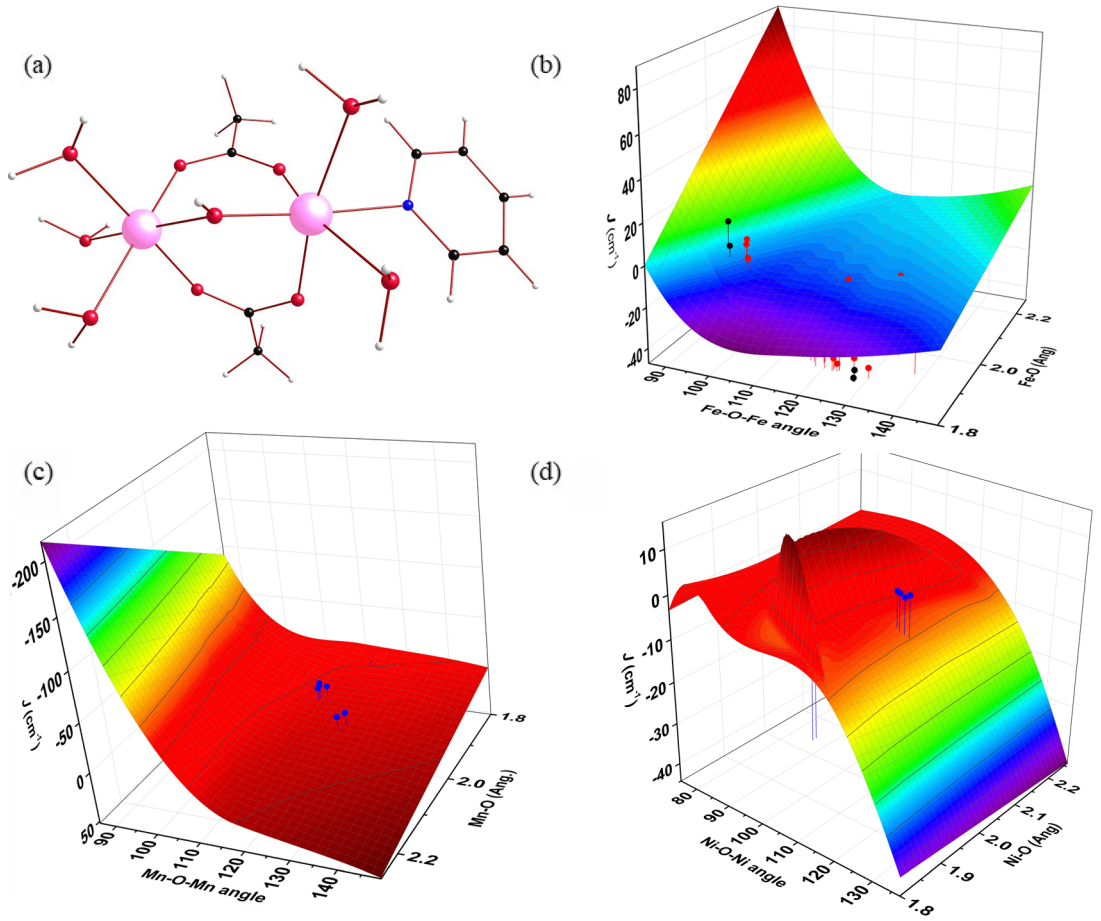

Figure 6. (a) Structures of model 1 employed in the magneto-structural correlation. Contour plot showing magneto-structural correlation developed by varying M−O(μ_2)−M angle and M−O distance in model 1 for (b) Fe(III) dimer, (c) Mn(III) dimer, and (d) Ni(II) dimer. Red-colored, small solid sphere in b and blue-colored, small solid sphere in c and d represent DFT computed J values for complexes **1**−**6** that are superimposed on the correlation. Black solid sphere in b represents experimental J obtained on various polynuclear Fe^{III} complexes.[26a,14o,p]

develop a magneto-structural correlation on a model system (model 1) by varying simultaneously both the Fe(III)−O bond distance and the Fe−O−Fe bond angle (see Figure 6a). Similar models were also constructed for Mn(III) and Ni(II) systems to probe the effect of metal substitution on the estimated J's. These three-dimensional correlations developed are shown in Figure 6.

Magneto-structural studies performed on model 1 (see Figure 6b; the J calculated on this model is −17.2 cm^{-1} and the structural parameters for this model are the same as J_3 in complex **1** with a change in some of the coordinating ligands) suggest that the expected value of magnetic coupling varies between ∼+15 cm^{-1} and −30 cm^{-1} with a strong antiferromagnetic coupling found when the Fe−O−Fe angles are in the range of 111° to 127° and the Fe−O distances are 1.80−1.85 Å. Strong ferromagnetic couplings are detected only in a narrow range, when the Fe−O distances are relatively long (from 1.9 to 2.0 Å) and the Fe−O−Fe angles are very narrow (from 85° to 95°). Moderate antiferromagnetic coupling on the order of −30 cm^{-1} to −5 cm^{-1} is found to be widespread in the graph with larger structural variations. As the M−μ_2O−M angle decreases (see Figure 6), the antiferromagnetic nature of the magnetic coupling constant for the Fe(III)-model complex increases very slowly up to 103° and then decreases sharply below this value and attains a ferromagnetic nature below 90°. We have also performed overlap integral calculations, which suggest a very small interaction of magnetic orbitals between both Fe(III) centers below a 90 °Fe−O−Fe angle, leading to a ferromagnetic coupling. At an Fe−O−Fe angle of 94°, only one possible strong interaction ($d_{xz}|p_x|d_{xz}$) exists, leading to a small antiferromagnetic interaction. For points above 94°, relatively stronger interactions appear ($d_{x^2-y^2}|p_x|d_{xz}$, $d_{x^2-y^2}|p_x|d_{xy}$ and $d_{z^2}|p_x|d_{xy}$), which strengthen the antiferromagnetic J's until 119°, and above this threshold, the interactions again started to diminish (see Table S3a,b).

Clearly, in complexes **1**−**4**, the Fe−O(μ_3) bond distances are found to be in the range of 1.886−2.034 Å, and Fe−O(μ_2)−Fe bond angles are found in the range of 97−132°. The computed J's and their variations are in line with the correlation developed. For example, the J_3 (or J_6) is the strongest interaction here, essentially due to a very short Fe−O distance and relatively large Fe−O−Fe angles. Similarly, the weakest interaction J_4 (or J_1) is essentially due to an acute Fe−O−Fe angle (100°, see Table 1) and a very long Fe−O distances. Thus, these two structural parameters influence the J's significantly not only in complex **1** but also in complexes **2**−**4**. The J_5 interactions computed for complex **4** are found to be ferromagnetic, and this is essentially due to a very long Fe−O distance and a very acute Fe−O−Fe angle, falling in the narrow range predicted in our correlations (Fe−O distance 1.945 Å and Fe−O−Fe angle 99°). Among all the iron complexes **1**−**4**, the strongest antiferromagnetic exchange was

DOI: 10.1021/acs.inorgchem.8b03257
Inorg. Chem. 2019, 58, 3175−3188

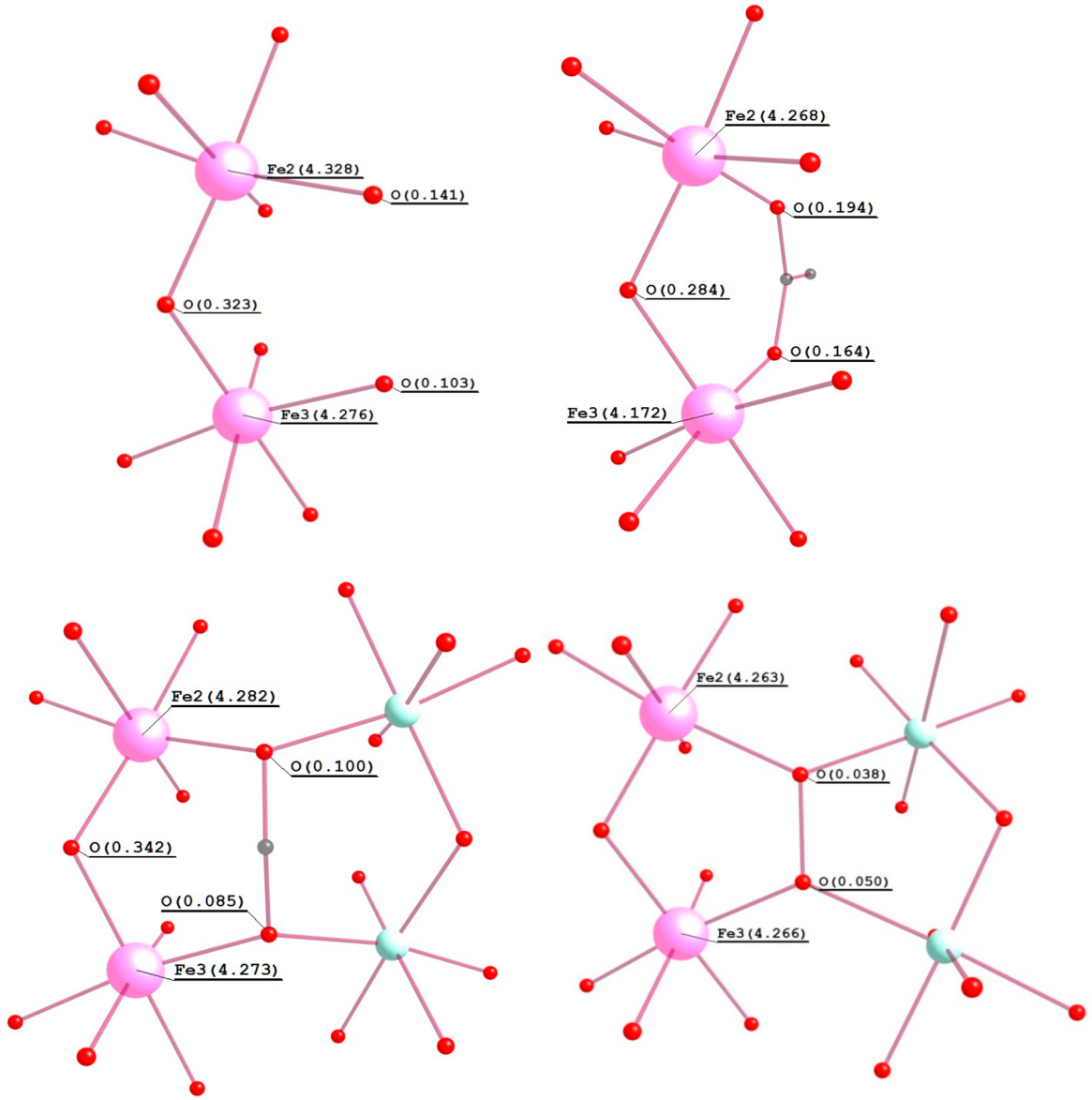

Figure 7. Structures of models 2−5 along with the computed spin densities on selected atoms. Magnetic coupling values for models 2−5 are calculated to be −20.1 cm^{-1}, −5.9 cm^{-1}, −20.8 cm^{-1}, and −24.3 cm^{-1}, respectively.

computed to be the J_4 interaction in complex **4**, and here, as one can expect, the Fe−O distances are very short coupled with a larger Fe−O−Fe angle (Fe−O distance 1.891 Å and Fe−O−Fe −123°), leading to very strong antiferromagnetic coupling.

Magneto-structural correlation developed for the Mn(III) model unveils a much wider J range; however, very strong antiferromagnetic couplings are found only when Mn−O−Mn angles are very small (less than 100°) with much more stringent and narrower Mn−O distances (see Figure 6c). Moderate antiferromagnetic and ferromagnetic couplings are widespread in the graph covering larger structural variations. In the Mn(III) model, the antiferromagnetic coupling constant increases slowly with the decrease in Mn−O(μ_2)−Mn angle up to 119°. Below 119°, it increases very drastically and becomes strongly antiferromagnetic in nature. In complex **5**, the J_4 interaction is found to be strongly antiferromagnetic, and the J_2 interaction is found to be weakly ferromagnetic. This is correlated with a longer Mn−O distance and shorter Mn−O−Mn angles and a shorter Mn−O distance and wider Mn−O−Mn angles, respectively. Overlap calculations suggest strong and greater numbers of magnetic orbital interactions at the lower Mn−O−Mn angle and smaller Mn−O distances ($d_{xz}|p_x|d_{xy}$, $d_{xz}|p_x|d_{xz}$, and $d_{z^2}|p_x|d_{xz}$), and as the Mn−O−Mn angle and Mn−O distances increase, these interactions start to diminish (see Table S3c,d), rationalizing the observed behavior.

Magneto-structural correlation developed for the Ni(II) model system reveals that stronger antiferromagnetic coupling is generally observed here only when the Ni−O−Ni angles are larger than 125°, however, for a wider range of Ni−O distances. Moderate ferromagnetic coupling (between 4 cm^{-1} and 10 cm^{-1}) is found only in a narrow range of angles (92−101°) and Ni−O distances (1.87 to 1.96 Å), though weak ferromagnetic coupling is possible even if the parameter deviates slightly from the quoted narrow range. Overlap calculations suggest stronger and greater numbers of magnetic orbital interactions at a higher Ni−O−Ni angle ($d_{z^2}|p_x|d_{x^2-y^2}$, $d_{x^2-y^2}|p_x|d_{z^2}$, and $d_{x^2-y^2}|p_x|d_{x^2-y^2}$), and as the Ni−O−Ni angle

DOI: 10.1021/acs.inorgchem.8b03257
Inorg. Chem. 2019, 58, 3175−3188

decreases, these interactions start to diminish (Table S3e). Overlap integral calculations also suggest stronger $d_{z^2}|p_x|d_{x^2-y^2}$ interaction for Ni−O distance ranging between 2.03 and 2.14 Å (see Table S 3f). Above and below this range, the magnetic orbital interactions weaken. On the basis of the outcome of our magneto-structural studies (see Figure 6), we can say that among these two parameters, J more strongly depends on the M−O distance in Fe(III) complexes, whereas in the case of Mn(III) and Ni(II), the M−O−M angle was found to have a stronger influence on the estimated magnetic coupling.

It is important to note here that magneto-structural studies performed on these dimetallic models estimate magnetic coupling values which are in very good agreement with the DFT calculated magnetic coupling values for each dimetallic center in hexametallic complexes. This suggests that the structural parameters which control the magnetic coupling sign and magnitude in dimetallic complexes are the ones to control the same in the polymetallic complexes.

Role of Carboxylate Bridges in Mediating Exchange Coupling Constant. To understand the complementarity and counter-complementarity effect of bridging ligands in the magnetic coupling mechanism, we have constructed four more dinuclear model systems (models 2−5, see Figure 7a−d) keeping Fe2 and Fe3 magnetic centers and estimated the magnetic coupling constants. Model 2 has two Fe(III) centers bridged with one μ_2-OH group. To prove/disprove the counter-complementary effect of the carboxylate group (in the presence of μ_2-OH group), we have an additional μ_2-acetate group that bridges both Fe(III) centers (model 3). Models 4 and 5 are tetra-metallic models where we have kept only Fe2 and Fe3 paramagnetic centers and replaced the other two metallic centers with diamagnetic Co(III) metals. Models 4 and 5, along with one bridging μ_2-OH group, have one μ_4-($\eta_2\eta_2$-$CH_2O_2^{2-}$) and one μ_4-($\eta_2\eta_2$-O_2^{2-}) bridging group, respectively. Remaining valences are being saturated with water molecule in all these models. Models 4 and 5 suggest the extent of magnetic coupling mediated through both bridging groups (μ_4-($\eta_2\eta_2$-$CH_2O_2^{2-}$) and μ_4-($\eta_2\eta_2$-O_2^{2-})) within a trinuclear system.

In model 2, the computed J originates only from the bridging μ_2-OH group (J = −20.1 cm^{-1}). When one additional carboxylate group is included (model 3), the magnitude of the antiferromagnetic coupling decreases (J = −5.9 cm^{-1}), affirming the counter-complementarity phenomenon in these Fe(III) complexes.[36] When we replace these acetates with μ_4-($\eta_2\eta_2$-$CH_2O_2^{2-}$) and μ_4-($\eta_2\eta_2$-O_2^{2-}) groups, respectively, as in models 4 and 5, then the J values are found to be −20.8 cm^{-1} and −24.3 cm^{-1}, respectively. This suggests weaker complementarity contributions from these bridging groups. This clearly suggests that both oxalate and carbonate bridges only perturb the J values, while coupling two {Fe_3O} units, while the carboxylate-bridge alters the J values significantly. Thus, both oxalate or carbonate bridges are innocent in nature and can be utilized to build bigger architecture without significantly altering the exchange coupling constant of the building units. The overlap calculation on model 2 suggests three strong ($d_{z^2}|p_x|d_{xy}$, $d_{x^2-y^2}|p_x|d_{z^2}$, and $d_{xz}|p_x|d_{xz}$) and five intermediate magnetic orbital interactions ($d_{xy}|p_x|d_{z^2}$, $d_{x^2-y^2}|p_x|d_{xy}$, $d_{xy}|p_x|d_{x^2-y^2}$, $d_{x^2-y^2}|p_x|d_{x^2-y^2}$, and $d_{z^2}|p_x|d_{z^2}$; Table S4) giving a strong antiferromagnetic interaction between both Fe(III) centers. Whereas in model 3, only one strong magnetic orbital interaction ($d_{z^2}|p_x|d_{xy}$) is present giving weak antiferromagnetic interaction between both Fe(III) centers (see Table S4). Model 4 has the same number of strong ($d_{yz}|p_x|d_{xz}$, $d_{z^2}|p_x|d_{xz}$, and $d_{z^2}|p_x|d_{x^2-y^2}$) and intermediate magnetic orbital interactions ($d_{yz}|p_x|d_{yz}$, $d_{x^2-y^2}|p_x|d_{xy}$, $d_{x^2-y^2}|p_x|d_{z^2}$, $d_{x^2-y^2}|p_x|d_{x^2-y^2}$, and $d_{yz}|p_x|d_{z^2}$) as in model 2, yielding identical magnetic coupling constant values (see Table S4). In model 5, the number of strong magnetic interactions is found to be seven ($d_{xz}|p_x|d_{yz}$, $d_{xz}|p_x|d_{xy}$, $d_{xz}|p_x|d_{z^2}$, $d_{yz}|p_x|d_{xz}$, $d_{yz}|p_x|d_{z^2}$, $d_{x^2-y^2}|p_x|d_{z^2}$, and $d_{z^2}|p_x|d_{z^2}$) with only one intermediate interaction ($d_{z^2}|p_x|d_{xz}$), resulting in the strongest antiferromagnetic interaction for model 5 out of all studied models (see Table S4).

Probing the Origin of Zero-Field Splitting of S = 5 State in 1. For SMMs, besides the spin ground-state value (S_T), the zero-field splitting (zfs) parameters are other important parameters that control the energy barrier for spin reversal. Out of all studied hexametallic complexes, only complex **1** has a nonzero ground-spin state. Elaborate EPR and magnetic studies on complex **1** reveal $D_{S=5}$ to be −0.22 cm^{-1} for complex **1**.[14a] Our DFT calculations yield a D value of the S_T = 5 state to be −0.20 cm^{-1} along with an E value of −0.03 cm^{-1}, which is in good agreement with respect to the experimental D. Using the broken symmetry approach, the ground spin-state configuration described in Figure 2a is computed, and its corresponding spin−spin and spin−orbit contributions to D are estimated. Various contributions to the estimated D values are given in Table 3. The largest negative D contribution found to arise from SOMO to SOMO ($\alpha \rightarrow \beta$) excitations (−0.13 cm^{-1}), and this is essentially inter-Fe electron transfer. For example, the Fe(1) ion with an α-spin electron can exchange electron to Fe(2)/Fe(3) ion which possesses a β-hole. Additionally, there are also significant contributions from DOMO to VMO ($\beta \rightarrow \alpha$) excitations (total contribution −0.09 cm^{-1}) to the overall D value (see Table 3).

Table 3. Various Contributions to the $D_{S=5}$ and E Computed for Complex 1

excitations[a]	$D_{S=5}$, cm^{-1}	E, cm^{-1}
SOMO → VMO (alpha → alpha)	0.02	−0.01
DOMO → SOMO (beta → beta)	0.02	−0.00
SOMO → SOMO (alpha → beta)	−0.13	−0.02
DOMO → VMO (beta → alpha)	−0.09	0.00

[a]DOMO = doubly occupied molecular orbital, SOMO = singly occupied molecular orbital, VMO = virtual molecular orbital.

To further understand the origin of magnetic anisotropy in complex **1**, we have computed the single-ion anisotropy of all the Fe(III) centers, and these values are Fe(1), +0.37 cm^{-1}; Fe(2), −0.05 cm^{-1}; Fe(3), +0.12 cm^{-1}; Fe(4), +0.37 cm^{-1}; Fe(5), +0.19 cm^{-1}; Fe(6), +0.13 cm^{-1} (see Table S5 in the Supporting Information for various contributions to these D values). As expected, all the computed D values are very small; however, the magnitude and also sign (in one case) vary across different Fe centers. This is essentially due to varying structural distortions present around the Fe(III) center that influence the single-ion zfs, as has been noted by us earlier.[16a,37]

Now that the single-ion D is available in the next step, we aim to obtain the exchange anisotropy contribution to the $D_{S=5}$ ground state. Overall, $D_{S=5}$ has various contributions that are given in eq 3 (assuming collinearity among various contributions):

DOI: 10.1021/acs.inorgchem.8b03257
Inorg. Chem. 2019, 58, 3175−3188

$$D = d_1D_{Fe1} + d_2D_{Fe2} + d_3D_{Fe3} + d_4D_{Fe4} + d_5D_{Fe5} + d_6D_{Fe6} + 2d_{12}D_{Fe1Fe2} + 2d_{23}D_{Fe2Fe3} + 2d_{13}D_{Fe1Fe3} + 2d_{45}D_{Fe4Fe5} + 2d_{56}D_{Fe5Fe6} + 2d_{46}D_{Fe4Fe6} + 2d_{35}D_{Fe3Fe5} + 2d_{26}D_{Fe2Fe6} \quad (3)$$

Here, d_{1-6} are corresponding single-ion D coefficients, and d_{12-26} are coefficients corresponding to exchange coupled terms. These coefficients are estimated using the Genio program suite. We have used the same Hamiltonian as mentioned in eq 2a for complex **1** to estimate all the coefficients (see Table S5). If we can add the contributions arising from the exchange anisotropy, eq 3 becomes eq 4:

$$D = d_1D_{Fe1} + d_2D_{Fe2} + d_3D_{Fe3} + d_4D_{Fe4} + d_5D_{Fe5} + d_6D_{Fe6} + 8 \times 2 \times 0.200D_{FeFe} \quad (4)$$

Utilizing the computed single-ion D values (see Table S5) and the $D_{S=5}$ that is computed for the full cluster, the exchange anisotropy (D_{FeFe}) value can be extracted, and in the present case this turns out to be -0.115 cm^{-1}. Interestingly, our calculations reveal that the ground state $D_{S=5}$ is negative essentially due to significant negative D contribution arising from exchange anisotropy, as all the single ion anisotropies are estimated to be either positive or close to zero. Here, the exchange anisotropy arises due to the specific electronic configuration with four-spin-up Fe(III) centers and two-spin-down centers allowing possible intra-Fe exchange. A similar scenario was witnessed earlier for a $\{Cr_{12}\}$ cluster.[38]

CONCLUSIONS

Probing the magnetic exchange coupling constants and how they are altered by structural variations in large clusters is of great significance in the area of SMMs. Here, using density functional methods, we have studied six different hexanuclear clusters having the general structural motif of $\{M_6O_2\}$ with M being Fe(III), Mn(III), and Ni(II). Conclusions derived from this work are summarized below.

The B3LYP/TZV method employed yielded a good numerical estimate of J values in all six complexes. Particularly, our calculated J's not only reproduce the experimental susceptibility data but also correctly predict $S_T = 5$ ground state for complex **1** and $S_T = 0$ for others.

Calculations yield various J's for four $\{Fe_6\}$ clusters studied, and spin frustration within the $\{Fe_3O\}$ triangle due to strong and equal antiferromagnetic exchange lead to a diamagnetic ground state. If asymmetry is induced in the $\{Fe_3O\}$ triangle using targeted structural distortions or additional bridges, which offers complementarity/counter-complementarity effects, this may lead to noncompeting J's, which results in a nonzero spin ground state. Particularly, the peripheral exchange coupling constants are found to significantly influence the nature of the spin ground state.

For the $\{Mn_6O_2\}$ cluster, the exchange coupling constants are found to be weakly antiferromagnetic within the $\{Mn_3O\}$ unit, and a stronger intertriangle antiferromagnetic coupling leads to a diamagnetic ground state. For the $\{Ni_6(OH)_2\}$ cluster, on other hand, all the intratriangle magnetic couplings are ferromagnetic, but the intertriangle couplings are antiferromagnetic, resulting in again a diamagnetic ground state.

Extensive magneto-structural correlation developed on a model system corresponding to the J's present in these clusters reveals that, in the case of Fe(III), both the Fe−O distance and Fe−O−Fe angle play a proactive role in controlling the sign and strength of J's, while for Mn(III) and Ni(III), the M−O−M angle dictates the sign and strength of the J's. Despite a complex nature of the cluster structural parameters, developed correlation clearly reveals that it is still possible to rationalize both the sign and magnitude of J's in these clusters using the structural parameters that govern the exchange coupling constants. Thus, the discussion surrounding the magneto-structural correlations is transferable to other related large clusters, and one can utilize such plots to rationalize the J's obtained from the fits. This is extremely important as often there are several J's present, and it is difficult to obtain a unique set of J's that fit the susceptibility data.

DFT calculations are used to estimate the zero-field splitting parameter of $D_{S=5}$, and the value estimated corroborates well with the experimental value (-0.20 cm^{-1} vs -0.22 cm^{-1}). Additionally, using a breakdown approach, we have estimated the exchange contribution to this D value. Interestingly, the sign of D was found to be dictated by the exchange anisotropy as single-ion D values are found to be positive or zero.

To this end, our study in these clusters reveal that the alteration of peripheral structural parameters in these clusters may pave the way forward to fine-tune both the ground state S_T value and the corresponding magnetic anisotropy—a much sought after combination in the area of SMMs.

ASSOCIATED CONTENT

Supporting Information

The Supporting Information is available free of charge on the ACS Publications website at DOI: 10.1021/acs.inorgchem.8b03257.

Simulated susceptibility plots, Eigenvalue plots for trinuclear systems, computed spin configurations, spin density table, overlap integrals, and ZFS of single ion along with corresponding coefficients computed (PDF)

AUTHOR INFORMATION

Corresponding Author

*E-mail: rajaraman@chem.iitb.ac.in.

ORCID

Gopalan Rajaraman: 0000-0001-6133-3026

Notes

The authors declare no competing financial interest.

ACKNOWLEDGMENTS

G.R. would like to acknowledge the financial support from SERB-DST (EMR/2014/000247) India, and IIT Bombay for the high performance computing facility. M.K.S. would like to thank IIT Bombay for financial assistance. We would also like to thank Prof. D. Gatteschi and Prof. L. Sorace, University of Florence, for providing the Genio code.

REFERENCES

(1) (a) Dasgupta, S.; Bhattacharya, P. K.; Chattopadhyay, G.; Fukuoka, M.; Banerjee, H.; Roy, S. Genetic reinterpretation of crystallographicintergrowths of jacobsite andhausmannite from natural assemblages. *Mineral. Petrol.* **1987**, *37*, 109. (b) Ammala, P. S.; Batten, S. R.; Cashion, J. D.; Kepert, C. M.; Moubaraki, B.; Murray, K. S.; Spiccia, L.; West, B. O. Synthesis, molecular structure

DOI: 10.1021/acs.inorgchem.8b03257
Inorg. Chem. 2019, 58, 3175−3188

and magnetic properties of [Fe6(μ3-O)2(OPri)2(μ-OPri)6(O2CPh)-2(μ-O2CPh)4]. *Inorg. Chim. Acta* **2002**, *331*, 90. (c) Stamatatos, T. C.; Christou, A. G.; Mukherjee, S.; Poole, K. M.; Lampropoulos, C.; Abboud, K. A.; O'Brien, T. A.; Christou, G. High-Yield Syntheses and Reactivity Studies of Fe10 "Ferric Wheels": Structural, Magnetic, and Computational Characterization of a Star-Shaped Fe8 Complex. *Inorg. Chem.* **2008**, *47*, 9021. (d) Post, J. E. Manganese oxide minerals: Crystal structures and economic and environmental significance. *Proc. Natl. Acad. Sci. U. S. A.* **1999**, *96*, 3447.

(2) (a) Kurtz, D. M. Oxo- and hydroxo-bridged diiron complexes: a chemical perspective on a biological unit. *Chem. Rev.* **1990**, *90*, 585. (b) Lippard, S. J. Oxo-Bridged Polyiron Centers in Biology and Chemistry. *Angew. Chem., Int. Ed. Engl.* **1988**, *27*, 344. (c) Toftlund, H.; Murray, K. S.; Zwack, P. R.; Taylor, L. F.; Anderson, O. P. Structural and electronic properties of tetranuclear iron(III) pyridylamine complexes containing cofacial pairs of μ-oxo-bis(μ-acetato)-iron(III) moieties. Models for met hemerythrins. *J. Chem. Soc., Chem. Commun.* **1986**, 191. (d) Wilkins, P. C.; Wilkins, R. G. The coordination chemistry of the binuclear iron site in hemerythrin. *Coord. Chem. Rev.* **1987**, *79*, 195. (e) Vincent, J. B.; Huffman, J. C.; Christou, G.; Li, Q.; Nanny, M. A.; Hendrickson, D. N.; Fong, R. H.; Fish, R. H. Modeling the dinuclear sites of iron biomolecules: synthesis and properties of Fe2O(OAc)2Cl2(bipy)2 and its use as an alkane activation catalyst. *J. Am. Chem. Soc.* **1988**, *110*, 6898. (f) Bunker, G.; Petersson, L.; Sjoberg, B. M.; Sahlin, M.; Chance, M.; Chance, B.; Ehrenberg, A. Extended x-ray absorption fine structure studies on the iron-containing subunit of ribonucleotide reductase from Escherichia coli. *Biochemistry* **1987**, *26*, 4708. (g) Scarrow, R. C.; Maroney, M. J.; Palmer, S. M.; Que, L.; Roe, A. L.; Salowe, S. P.; Stubbe, J. EXAFS studies of binuclear iron proteins: hemerythrin and ribonucleotide reductase. *J. Am. Chem. Soc.* **1987**, *109*, 7857. (h) Sjoberg, B. M.; Sanders-Loehr, J.; Loehr, T. M. Identification of a hydroxide ligand at the iron center of ribonucleotide reductase by resonance Raman spectroscopy. *Biochemistry* **1987**, *26*, 4242. (i) Prince, R. C.; George, G. N.; Savas, J. C.; Cramer, S. P.; Patel, R. N. Spectroscopic properties of the hydroxylase of methane monooxygenase. *Biochim. Biophys. Acta, Protein Struct. Mol. Enzymol.* **1988**, *952*, 220. (j) Ericson, A.; Hedman, B.; Hodgson, K. O.; Green, J.; Dalton, H.; Bentsen, J. G.; Beer, R. H.; Lippard, S. J. Structural characterization by EXAFS spectroscopy of the binuclear iron center in protein A of methane monooxygenase from Methylococcus capsulatus (Bath). *J. Am. Chem. Soc.* **1988**, *110*, 2330. (k) Dalton, H. Oxidation of hydrocarbons by methane monooxygenases from a variety of microbes. *Adv. Appl. Microbiol.* **1980**, *26*, 71. (l) Woodland, M. P.; Dalton, H. Purification and characterization of component A of the methane monooxygenase from Methylococcus capsulatus (Bath). *J. Biol. Chem.* **1984**, *259*, 53. (m) Taft, K. L.; Papaefthymiou, G. S.; Lippard, S. J. A mixed-valent polyiron oxo complex that models the biomineralization of the ferritin core. *Science* **1993**, *259*, 1302. (n) Gorun, S. M.; Papaefthymiou, G. S.; Frankel, R. B.; Lippard, S. J. Synthesis, structure, and magnetic and Moessbauer properties of mononuclear and asymmetric, oxo-bridged trinuclear iron(III) complexes of a new polyimidazole ligand. *J. Am. Chem. Soc.* **1987**, *109*, 4244. (o) Yan, B.; Chen, Z. D. A novel tetranuclear iron complex [Fe4O2(O2CC2H5)7(bipy)2]PF6·2H2O (bipy = 2,2′-bipyridine): crystal structure and magnetic property. *Inorg. Chem. Commun.* **2001**, *4*, 138.

(3) (a) Theil, E. C. Ferritin: Structure, Gene Regulation, and Cellular Function in Animals, Plants, and Microorganisms. *Annu. Rev. Biochem.* **1987**, *56*, 289. (b) Xu, B.; Chasteen, N. D. Iron oxidation chemistry in ferritin. Increasing Fe/O2 stoichiometry during core formation. *J. Biol. Chem.* **1991**, *266*, 19965. (c) Theil, E. C.; Matzapetakis, M.; Liu, X. Ferritins: iron/oxygen biominerals in protein nanocages. *JBIC, J. Biol. Inorg. Chem.* **2006**, *11*, 803. (d) Grant, R. A.; Filman, D. J.; Finkel, S. E.; Kolter, R.; Hogle, J. M. The crystal structure of Dps, a ferritin homolog that binds and protects DNA. *Nat. Struct. Biol.* **1998**, *5*, 294.

(4) (a) Ovcharenko, V.; Fursova, E.; Romanenko, G.; Ikorskii, V. Synthesis and Structure of Heterospin Compounds Based on the [Mn6(O)2Piv10]-Cluster Unit and Nitroxide. *Inorg. Chem.* **2004**, *43*, 3332. (b) Eppley, H. J.; deVries, N.; Wang, S.; Aubin, S. M.; Tsai, H.-L.; Folting, K.; Hendrickson, D. N.; Christou, G. [Mn3O(O2CPh)-6(py)2]2(4,4′-bpy) and [Mn9O7(O2CC6H4-p-OMe)13 (4,4′-bpy)]2: new multinuclear manganese complexes. *Inorg. Chim. Acta* **1997**, *263*, 323. (c) Fursova, E.; Ovcharenko, V.; Nosova, K.; Romanenko, G.; Ikorskii, V. Heterospin compounds based on the [Mn6(O)2Piv10] cluster unit and nitroxides. *Polyhedron* **2005**, *24*, 2084.

(5) (a) Çelenligil-Çetin, R.; Staples, R. J.; Stavropoulos, P. Synthesis, Characterization, and Reactivity of Ferrous and Ferric Oxo/Peroxo Pivalate Complexes in Relation to Gif-Type Oxygenation of Substrates. *Inorg. Chem.* **2000**, *39*, 5838. (b) Eremenko, I. L.; Nefedov, S. E.; Sidorov, A. A.; Golubnichaya, M. A.; Danilov, P. V.; Ikorskii, V. N.; Shvedenkov, Y. G.; Novotortsev, V. M.; Moiseev, I. I. Bi- and Mononuclear Nickel(II) Trimethylacetate Complexes with Pyridine Bases as Ligands. *Inorg. Chem.* **1999**, *38*, 3764. (c) Barton, D. H. R.; Doller, D. The selective functionalization of saturated hydrocarbons: Gif chemistry. *Acc. Chem. Res.* **1992**, *25*, 504.

(6) (a) Sañudo, E. C.; Grillo, V. A.; Yoo, J.; Huffman, J. C.; Bollinger, J. C.; Hendrickson, D. N.; Christou, G. Synthesis, structural characterization and magnetic properties of mixed-valent bis-bipyridine manganese carboxylate clusters. *Polyhedron* **2001**, *20*, 1269. (b) Hill, S.; Edwards, R. S.; Aliaga-Alcalde, N.; Christou, G. Quantum Coherence in an Exchange-Coupled Dimer of Single-Molecule Magnets. *Science* **2003**, *302*, 1015. (c) Sessoli, R.; Gatteschi, D.; Caneschi, A.; Novak, M. A. MAGNETIC BISTABILITY IN A METAL-ION CLUSTER. *Nature* **1993**, *365*, 141. (d) Sessoli, R.; Tsai, H. L.; Schake, A. R.; Wang, S.; Vincent, J. B.; Folting, K.; Gatteschi, D.; Christou, G.; Hendrickson, D. N. High-spin molecules: [Mn12O12(O2CR)16(H2O)4]. *J. Am. Chem. Soc.* **1993**, *115*, 1804. (e) Jones, L. F.; Brechin, E. K.; Collison, D.; Helliwell, M.; Mallah, T.; Piligkos, S.; Rajaraman, G.; Wernsdorfer, W. **A** Novel Undecametallic Iron(III) Cluster with an $S = {}^{11}/_{2}$ Spin Ground State. *Inorg. Chem.* **2003**, *42*, 6601. (f) Powell, A. K.; Heath, S. L.; Gatteschi, D.; Pardi, L.; Sessoli, R.; Spina, G.; Del Giallo, F.; Pieralli, F. Synthesis, Structures, and Magnetic Properties of Fe2, Fe17, and Fe19 Oxo-Bridged Iron Clusters: The Stabilization of High Ground State Spins by Cluster Aggregates. *J. Am. Chem. Soc.* **1995**, *117*, 2491. (g) McCusker, J. K.; Vincent, J. B.; Schmitt, E. A.; Mino, M. L.; Shin, K.; Coggin, D. K.; Hagen, P. M.; Huffman, J. C.; Christou, G.; Hendrickson, D. N. Molecular spin frustration in the [Fe4O2]8+ core: synthesis, structure, and magnetochemistry of tetranuclear iron-oxo complex [Fe4O2(O2CR)7(bpy)2](C1O4) (R = Me, Ph). *J. Am. Chem. Soc.* **1991**, *113*, 3012. (h) Kahn, O. Competing spin interactions and degenerate frustration for discrete molecular species. *Chem. Phys. Lett.* **1997**, *265*, 109. (i) Bagai, R.; Datta, S.; Betancur-Rodriguez, A.; Abboud, K. A.; Hill, S.; Christou, G. Diversity of New Structural Types in Polynuclear Iron Chemistry with a Tridentate N,N,O Ligand. *Inorg. Chem.* **2007**, *46*, 4535. (j) Bagai, R.; Abboud, K. A.; Christou, G. A New N,N,O Chelate for Transition Metal Chemistry: Fe_5 and Fe_6Clusters from the Use of 6-Hydroxymethyl-2,2′-bipyridine (hmbpH). *Inorg. Chem.* **2007**, *46*, 5567.

(7) (a) Christou, G. Single-molecule magnets: a molecular approach to nanoscale magnetic materials. *Polyhedron* **2005**, *24*, 2065. (b) Aromí, G.; Brechin, E. K. Synthesis of 3d metallic single-molecule magnets. *Struct. Bonding (Berlin)* **2006**, *122*, 1.

(8) (a) Christou, G.; Gatteschi, D.; Hendrickson, D. N.; Sessoli, R. Single-molecule magnets. *MRS Bull.* **2000**, *25*, 66. (b) Sun, Z.; Ruiz, D.; Rumberger, E.; Incarvito, C. D.; Folting, K.; Rheingold, A. L.; Christou, G.; Hendrickson, D. N. Isomeric Forms of [Mn12O12-(O2CR)16(H2O)4] Single-Molecule Magnets. *Inorg. Chem.* **1998**, *37*, 4758. (c) Gatteschi, D.; Sessoli, R.; Cornia, A. Single-molecular magnets based on iron(III) oxo-clusters. *Chem. Commun.* **2000**, 725.

(9) Caneschi, A.; Gatteschi, D.; Sessoli, R.; Barra, A. L.; Brunel, L. C.; Guillot, n. Alternating current susceptibility, high field magnetization, and millimeter band EPR evidence for a ground S = 10 state in [Mn12O12(Ch3COO)16(H2O)4].2CH3COOH.4H2O. *J. Am. Chem. Soc.* **1991**, *113*, 5873.

DOI: 10.1021/acs.inorgchem.8b03257
Inorg. Chem. 2019, 58, 3175−3188

(10) (a) Weighardt, K.; Pohl, K.; Jibril, I.; Huttner, G. Hydrolysis Products of the Monomeric Amine Complex $(C_6H_{15}N_3)FeCl_3$: The Structure of the Octameric Iron(III) Cation of $\{[(C_6H_{15}N_3)_6Fe_8(\mu_3\text{-}O)_2(\mu_2\text{-}OH)_{12}]Br_7(H_2O)\}Br\cdot 8H_2O$. *Angew. Chem., Int. Ed. Engl.* **1984**, *23*, 77. (b) Delfs, C.; Gatteschi, D.; Pardi, L.; Sessoli, R.; Wieghardt, K.; Hanke, D. Magnetic properties of an octanuclear iron(III) cation. *Inorg. Chem.* **1993**, *32*, 3099. (c) Barra, A. L.; Gatteschi, D.; Sessoli, R. High-Frequency EPR Spectra of [Fe8O2-(OH)12(tacn)6]Br8: A Critical Appraisal of the Barrier for the Reorientation of the Magnetization in Single-Molecule Magnets. *Chem. - Eur. J.* **2000**, *6*, 1608.

(11) Goodwin, J. C.; Sessoli, R.; Gatteschi, D.; Wernsdorfer, W.; Powell, A. K.; Heath, S. L. Towards nanostructured arrays of single molecule magnets: new Fe_{19} oxyhydroxide clusters displaying high ground state spins and hysteresis. *Dalton Trans* **2000**, *12*, 1835.

(12) (a) Scheurer, A.; Gieb, K.; Alam, M. S.; Heinemann, F. W.; Saalfrank, R. W.; Kroener, W.; Petukhov, K.; Stocker, M.; Muller, P. Synthesis, magnetic properties, and STM spectroscopy of an unprecedented octanuclear chloro-bridged nickel(ii) double cubane. *Dalton Trans* **2012**, *41*, 3553. (b) Milios, C. J.; Vinslava, A.; Wernsdorfer, W.; Moggach, S.; Parsons, S.; Perlepes, S. P.; Christou, G.; Brechin, E. K. A Record Anisotropy Barrier for a Single-Molecule Magnet. *J. Am. Chem. Soc.* **2007**, *129*, 2754.

(13) Milios, C. J.; Inglis, R.; Vinslava, A.; Bagai, R.; Wernsdorfer, W.; Parsons, S.; Perlepes, S. P.; Christou, G.; Brechin, E. K. Toward a Magnetostructural Correlation for a Family of Mn6 SMMs. *J. Am. Chem. Soc.* **2007**, *129*, 12505.

(14) (a) Cooper, P.; Tuna, F.; Shanmugam, M.; Sorace, L.; Heath, S. L.; Collison, D.; McInnes, E. J. L.; Winpenny, R. E. P. Synthesis, structural, magnetic and high frequency EPR studies on a hexametallic Fe(III) complex with a highly rhombic ground state. *Inorg. Chim. Acta* **2008**, *361*, 3663. (b) Murugesu, M.; Abboud, K. A.; Christou, G. New hexanuclear and dodecanuclear Fe(III) clusters with carboxylate and alkoxide-based ligands from cluster aggregation reactions. *Polyhedron* **2004**, *23*, 2779. (c) Seddon, E. J.; Huffman, J. C.; Christou, G. A new core topology in hexanuclear iron(III) carboxylate chemistry: $[Fe_6O_3(O_2CMe)_9(OEt)_2(bpy)_2](ClO_4)$. *J. Chem. Soc., Dalton Trans.* **2000**, 4446. (d) Chakov, N. E.; Zakharov, L. N.; Rheingold, A. L.; Abboud, K. A.; Christou, G. New Polynuclear Manganese Clusters from the Use of the Hydrophobic Carboxylate Ligand 2,2-Dimethylbutyrate. *Inorg. Chem.* **2005**, *44*, 4555. (e) Ovcharenko, V.; Fursova, E.; Romanenko, G.; Eremenko, I.; Tretyakov, E.; Ikorskii, V. Synthesis, Structure, and Magnetic Properties of (6−9)-Nuclear Ni(II) Trimethylacetates and Their Heterospin Complexes with Nitroxides. *Inorg. Chem.* **2006**, *45*, 5338. (f) Cañada-Vilalta, C.; O'Brien, T. A.; Brechin, E. K.; Pink, M.; Davidson, E. R.; Christou, G. Large Spin Differences in Structurally Related Fe_6 Molecular Clusters and Their Magnetostructural Explanation. *Inorg. Chem.* **2004**, *43*, 5505. (g) Gass, I. A.; Milios, C. J.; Collins, A.; White, F. J.; Budd, L.; Parsons, S.; Murrie, M.; Perlepes, S. P.; Brechin, E. K. Polymetallic clusters of iron(iii) with derivatised salicylaldoximes. *Dalton Transactions* **2008**, 2043. (h) Taguchi, T.; Stamatatos, T. C.; Abboud, K. A.; Jones, C. M.; Poole, K. M.; O'Brien, T. A.; Christou, G. New Fe4, Fe6, and Fe8 Clusters of Iron(III) from the Use of 2-Pyridyl Alcohols: Structural, Magnetic, and Computational Characterization. *Inorg. Chem.* **2008**, *47*, 4095. (i) Bagai, R.; Daniels, M. R.; Abboud, K. A.; Christou, G. Unusual Structural Types in Polynuclear Iron Chemistry from the Use of N,N,N′,N′-Tetrakis(2-hydroxyethyl)ethylenediamine (edteH4): Fe5, Fe6, and Fe12 Clusters. *Inorg. Chem.* **2008**, *47*, 3318. (j) Lu, J.-W.; Lin, Y.-W.; Takahahsi, M.; Wei, H.-H. A novel hexanuclear iron(III) complex containing three-coordination symmetries with two bridging μ-alkoxo groups, two μ3-oxo and four μ-catecholato bridges. *Inorg. Chem. Commun.* **2008**, *11*, 388. (k) Baran, P.; Boča, R.; Chakraborty, I.; Giapintzakis, J.; Herchel, R.; Huang, Q.; McGrady, J. E.; Raptis, R. G.; Sanakis, Y.; Simopoulos, A. Synthesis, Characterization, and Study of Octanuclear Iron-Oxo Clusters Containing a Redox-Active Fe4O4-Cubane Core. *Inorg. Chem.* **2008**, *47*, 645. (l) Turner, D. R.; Pek, S. N.; Cashion, J. D.; Moubaraki, B.; Murray, K. S.; Batten, S. R. A sheet of clusters: self-assembly of a (4,4) network of FeIII10clusters. *Dalton Trans* **2008**, 6877. (m) McDonald, C.; Sanz, S.; Brechin, E. K.; Singh, M. K.; Rajaraman, G.; Gaynor, D.; Jones, L. F. High nuclearity Ni(ii) cages from hydroxamate ligands. *RSC Adv.* **2014**, *4*, 38182. (n) Çelenligil-Çetin, R.; Staples, R. J.; Stavropoulos, P. Synthesis, Characterization, and Reactivity of Ferrous and Ferric Oxo/Peroxo Pivalate Complexes in Relation to Gif-Type Oxygenation of Substrates. *Inorg. Chem.* **2000**, *39*, 5838. (o) Mitchell, K. J.; Abboud, K. A.; Christou, G. Magnetostructural Correlation for High Nuclearity Iron(III)/oxo Complexes, and Application to Fe5, Fe6 and Fe8. *Inorg. Chem.* **2016**, *55*, 6597. (p) Overgaard, J.; Hibbs, D. E.; Rentschler, E.; Timco, G. A.; Larsen, F. K. Experimental and Theoretical Electron Density Distribution and Magnetic Properties of the Butterfly-like Complex $[Fe_4O_2(O_2CCMe_3)_8(NC_5H_4Me)_2]\cdot 2CH_3CN$. *Inorg. Chem.* **2003**, *42*, 7593.

(15) Kang, S.; Zheng, H.; Liu, T.; Hamachi, K.; Kanegawa, S.; Sugimoto, K.; Shiota, Y.; Hayami, S.; Mito, M.; Nakamura, T.; Nakano, M.; Baker, M. L.; Nojiri, H.; Yoshizawa, K.; Duan, C.; Sato, O. A ferromagnetically coupled Fe42 cyanide-bridged nanocage. *Nat. Commun.* **2015**, *6*, 5955.

(16) (a) Singh, S. K.; Gupta, T.; Badkur, P.; Rajaraman, G. Magnetic anisotropy of mononuclear NiII complexes: On the importance of structural diversity and the structural distortions. *Chem. - Eur. J.* **2014**, *20*, 10305. (b) Craig, G. A.; Sarkar, A.; Woodall, C. H.; Hay, M. A.; Marriott, K. E. R.; Kamenev, K. V.; Moggach, S. A.; Brechin, E. K.; Parsons, S.; Rajaraman, G.; Murrie, M. Probing the origin of the giant magnetic anisotropy in trigonal bipyramidal Ni(ii) under high pressure. *Chem. Sci.* **2018**, *9*, 1551.

(17) (a) Barros, W. P.; Inglis, R.; Nichol, G. S.; Rajeshkumar, T.; Rajaraman, G.; Piligkos, S.; Stumpf, H. O.; Brechin, E. K. From antiferromagnetic to ferromagnetic exchange in a family of oxime-based MnIII dimers: A magneto-structural study. *Dalton Trans* **2013**, *42*, 16510. (b) Berg, N.; Rajeshkumar, T.; Taylor, S. M.; Brechin, E. K.; Rajaraman, G.; Jones, L. F. What controls the magnetic interaction in bis-μ-alkoxo Mn III dimers? A combined experimental and theoretical exploration. *Chem. - Eur. J.* **2012**, *18*, 5906.

(18) Cirera, J.; Jiang, Y.; Qin, L.; Zheng, Y. Z.; Li, G.; Wu, G.; Ruiz, E. Ferromagnetism in polynuclear systems based on non-linear [Mn II 2 MnIII] building blocks. *Inorg. Chem. Front.* **2016**, *3*, 1272.

(19) (a) Aravena, D.; Venegas-Yazigi, D.; Ruiz, E. Exchange Interactions on the Highest-Spin Reported Molecule: the Mixed-Valence Fe42 Complex. *Sci. Rep.* **2016**, *6*, 23847. (b) Ako, A. M.; Hewitt, I. J.; Mereacre, V.; Clérac, R.; Wernsdorfer, W.; Anson, C. E.; Powell, A. K. A Ferromagnetically Coupled Mn19 Aggregate with a Record S = 83/2 Ground Spin State. *Angew. Chem., Int. Ed.* **2006**, *45*, 4926.

(20) (a) Grant, C. M.; Knapp, M. J.; Huffman, J. C.; Hendrickson, D. N.; Christou, G.; Streib, W. E. Dinuclear and Hexanuclear Iron(III) Oxide Complexes with a Bis(bipyridine) Ligand: A New $[Fe_6(\mu_3\text{-}O)_4]^{10+}$ Core. *Inorg. Chem.* **1998**, *37*, 6065. (b) Nair, V. S.; Hagen, K. S. Iron oxo aggregation: Fe3 to Fe6. Synthesis, structure, and magnetic properties of the hexanuclear dication [Fe6(.mu.4-O)2(.mu.2-OMe)8(OMe)4(tren)2]2+, a soluble, crystalline model of iron oxo hydroxo nanoparticles, the core of ferritin and rust formation. *Inorg. Chem.* **1992**, *31*, 4048. (c) Cornia, A.; Gatteschi, D.; Hegetschweiler, K.; Hausherr-Primo, L.; Gramlich, V. Metal Binding of Polyalcohols. 4.† Structure and Magnetism of the Hexanuclear, μ_6-Oxo-Centered $[OFe_6(H_{-3}thme)_3(OCH_3)_3Cl_6]^{2-}$ (thme = 1,1,1-Tris(hydroxymethyl)ethane). *Inorg. Chem.* **1996**, *35*, 4414. (d) Cauchy, T.; Ruiz, E.; Alvarez, S. Exchange coupling interactions in a Fe_6 complex: A theoretical study using density functional theory. *Phys. B* **2006**, *384*, 116.

(21) Khanra, S.; Konar, S.; Clearfield, A.; Helliwell, M.; McInnes, E. J. L.; Tolis, E.; Tuna, F.; Winpenny, R. E. P. Synthesis, Structural and Magnetochemical Studies of Iron Phosphonate Cages Based on {Fe3O}7+ Core. *Inorg. Chem.* **2009**, *48*, 5338.

(22) Pladzyk, A.; Ponikiewski, Ł.; Lan, Y.; Powell, A. K. Synthesis, structure and magnetic properties of neutral Ni (II) tri-tert-butoxysilanethiolate cluster. *Inorg. Chem. Commun.* **2012**, *20*, 66.

DOI: 10.1021/acs.inorgchem.8b03257
Inorg. Chem. 2019, 58, 3175−3188

(23) Frisch, M. J.; Trucks, G. W.; Schlegel, H. B.; Scuseria, G. E.; Robb, M. A.; Cheeseman, J. R.; Scalmani, G.; Barone, V.; Mennucci, B.; Petersson, G. A.; Nakatsuji, H.; Caricato, M.; Li, X.; Hratchian, H. P.; Izmaylov, A. F.; Bloino, J.; Zheng, G.; Sonnenberg, J. L.; Hada, M.; Ehara, M.; Toyota, K.; Fukuda, R.; Hasegawa, J.; Ishida, M.; Nakajima, T.; Honda, Y.; Kitao, O.; Nakai, H.; Vreven, T.; Montgomery, J. A.; Peralta, J. E.; Ogliaro, F.; Bearpark, M.; Heyd, J. J.; Brothers, E.; Kudin, K. N.; Staroverov, V. N.; Kobayashi, R.; Normand, J.; Raghavachari, K.; Rendell, A.; Burant, J. C.; Iyengar, S. S.; Tomasi, J.; Cossi, M.; Rega, N.; Millam, J. M.; Klene, M.; Knox, J. E.; Cross, J. B.; Bakken, V.; Adamo, C.; Jaramillo, J.; Gomperts, R.; Stratmann, R. E.; Yazyev, O.; Austin, A.; Cammi, J. R.; Pomelli, C.; Ochterski, J. W.; Martin, R. L.; Morokuma, K.; Zakrzewski, V. G.; Voth, G. A.; Salvador, P.; Dannenberg, J. J.; Dapprich, S.; Daniels, A. D.; Farkas, Ö.; Foresman, J. B.; Ortiz, J. V.; Cioslowski, J.; Fox, D. J. *Gaussian 09*; Gaussian Inc., 2009.

(24) (a) Lee, C.; Yang, W.; Parr, R. G. Development of the Colle-Salvetti correlation-energy formula into a functional of the electron density. *Phys. Rev. B: Condens. Matter Mater. Phys.* **1988**, *37*, 785. (b) Becke, A. D. Density-functional thermochemistry. III. The role of exact exchange. *J. Chem. Phys.* **1993**, *98*, 5648. (c) Becke, A. D. A new mixing of Hartree−Fock and local density-functional theories. *J. Chem. Phys.* **1993**, *98*, 1372. (d) Stephens, P. J.; Devlin, F. J.; Chabalowski, C. F.; Frisch, M. J. Ab Initio Calculation of Vibrational Absorption and Circular Dichroism Spectra Using Density Functional Force Fields. *J. Phys. Chem.* **1994**, *98*, 11623.

(25) (a) Schaefer, A.; Horn, H.; Ahlrichs, R. Fully optimized contracted Gaussian basis sets for atoms Li to Kr. *J. Chem. Phys.* **1992**, *97*, 2571. (b) Schaefer, A.; Huber, C.; Ahlrichs, R. Fully optimized contracted Gaussian basis sets of triple zeta valence quality for atoms Li to Kr. *J. Chem. Phys.* **1994**, *100*, 5829. (c) Scuseria, G. E.; Schaefer, H. F., III Is coupled cluster singles and doubles (CCSD) more computationally intensive than quadratic configuration interaction (QCISD)? *J. Chem. Phys.* **1989**, *90*, 3700.

(26) (a) Cauchy, T.; Ruiz, E.; Alvarez, S. Magnetostructural Correlations in Polynuclear Complexes: The Fe4 Butterflies. *J. Am. Chem. Soc.* **2006**, *128*, 15722. (b) Tolis, E. I.; Engelhardt, L. P.; Mason, P. V.; Rajaraman, G.; Kindo, K.; Luban, M.; Matsuo, A.; Nojiri, H.; Raftery, J.; Schröder, C.; Timco, G. A.; Tuna, F.; Wernsdorfer, W.; Winpenny, R. E. P. Studies of an Fe9 Tridiminished Icosahedron. *Chem. - Eur. J.* **2006**, *12*, 8961. (c) Rajaraman, G.; Sañudo, E. C.; Helliwell, M.; Piligkos, S.; Wernsdorfer, W.; Christou, G.; Brechin, E. K. Magnetic and theoretical characterization of a ferromagnetic Mn(III) dimer. *Polyhedron* **2005**, *24*, 2450. (d) Gupta, T.; Rajaraman, G. Modelling spin Hamiltonian parameters of molecular nanomagnets. *Chem. Commun.* **2016**, *52*, 8972.

(27) (a) Noodleman, L.; Norman, J. G. The *Xα* valence bond theory of weak electronic coupling. Application to the low-lying states of $Mo_2Cl_8^{4-}$. *J. Chem. Phys.* **1979**, *70*, 4903. (b) Noodleman, L. Valence bond description of antiferromagnetic coupling in transition metal dimers. *J. Chem. Phys.* **1981**, *74*, 5737. (c) Noodleman, L.; Davidson, E. R. Ligand spin polarization and antiferromagnetic coupling in transition metal dimers. *Chem. Phys.* **1986**, *109*, 131. (d) Noodleman, L.; Case, D. A. Density-Functional Theory of Spin Polarization and Spin Coupling in Iron—Sulfur Clusters. *Adv. Inorg. Chem.* **1992**, *38*, 423.

(28) Kobayashi, K.; Sano, Y.; Nagase, S. AIM2000. *J. Comput. Chem.* **2001**, *22*, 1353.

(29) Borras-Almenar, J. J.; Clemente-Juan, J. M.; Coronado, E.; Tsukerblat, B. S. MAGPACK[1] A package to calculate the energy levels, bulk magnetic properties, and inelastic neutron scattering spectra of high nuclearity spin clusters. *J. Comput. Chem.* **2001**, *22*, 985.

(30) Caballero-Jiménez, J.; Habib, F.; Ramírez-Rosales, D.; Grande-Aztatzi, R.; Merino, G.; Korobkov, I.; Singh, M. K.; Rajaraman, G.; Reyes-Ortega, Y.; Murugesu, M. Inducing magnetic communication in caged dinuclear Co(ii) systems. *Dalton Trans* **2015**, *44*, 8649.

(31) (a) Cirera, J.; Ruiz, E.; Alvarez, S.; Neese, F.; Kortus, J. How to build molecules with large magnetic anisotropy. *Chem. - Eur. J.* **2009**, *15*, 4078. (b) Ruiz, E.; Cirera, J.; Cano, J.; Alvarez, S.; Loose, C.; Kortus, J. Can large magnetic anisotropy and high spin really coexist? *Chem. Commun.* **2008**, *0*, 52.

(32) (a) Neese, F.; Petrenko, T.; Ganyushin, D.; Olbrich, G. Advanced aspects of ab initio theoretical optical spectroscopy of transition metal complexes: Multiplets, spin-orbit coupling and resonance Raman intensities. *Coord. Chem. Rev.* **2007**, *251*, 288. (b) Neese, F. The ORCA program system. *Wiley Interdiscip. Rev. Comput. Mol. Sci.* **2012**, *2*, 73.

(33) Ganyushin, D.; Neese, F. First-principles calculations of zero-field splitting parameters. *J. Chem. Phys.* **2006**, *125*, 024103.

(34) Neese, F. Calculation of the zero-field splitting tensor on the basis of hybrid density functional and Hartree-Fock theory. *J. Chem. Phys.* **2007**, *127*, 164112.

(35) Weigend, F. Accurate Coulomb-fitting basis sets for H to Rn. *Phys. Chem. Chem. Phys.* **2006**, *8*, 1057.

(36) Hazra, S.; Bhattacharya, S.; Singh, M. K.; Carrella, L.; Rentschler, E.; Weyhermueller, T.; Rajaraman, G.; Mohanta, S. Syntheses, Structures, Magnetic Properties, and Density Functional Theory Magneto-Structural Correlations of Bis(*μ*-phenoxo) and Bis(*μ*-phenoxo)-*μ*-acetate/Bis(*μ*-phenoxo)-bis(*μ*-acetate) Dinuclear FeIIINiII Compounds. *Inorg. Chem.* **2013**, *52*, 12881.

(37) (a) Singh, S. K.; Rajaraman, G. Probing the origin of magnetic anisotropy in a dinuclear {Mn IIICuII} single-molecule magnet: The role of exchange anisotropy. *Chem. - Eur. J.* **2014**, *20*, 5214. (b) Singh, S. K.; Rajaraman, G. Can anisotropic exchange be reliably calculated using density functional methods? a case study on trinuclear MnIII-MIII-Mn III (M = Fe, Ru, and Os) cyanometalate single-molecule magnets. *Chem. - Eur. J.* **2014**, *20*, 113. (c) Caballero-Jimenez, J.; Habib, F.; Ramirez-Rosales, D.; Grande-Aztatzi, R.; Merino, G.; Korobkov, I.; Singh, M. K.; Rajaraman, G.; Reyes-Ortega, Y.; Murugesu, M. Inducing magnetic communication in caged dinuclear Co(ii) systems. *Dalton Trans* **2015**, *44*, 8649.

(38) Collison, D.; Oganesyan, V. S.; Piligkos, S.; Thomson, A. J.; Winpenny, R. E. P.; McInnes, E. J. L. Optical Determination of the Single-Ion Zero-Field Splitting in Large Spin Clusters. *J. Am. Chem. Soc.* **2003**, *125*, 1168.

DOI: 10.1021/acs.inorgchem.8b03257
Inorg. Chem. 2019, 58, 3175−3188